

RETURNING MATERIALS:
Place in book drop to remove this checkout from your record. FINES will be charged if book is returned after the date stamped below.

POLAROGRAPHIC DETERMINATION OF THE NORMAL

INTRARETINAL OXYGEN TENSION OF THE

RAINBOW TROUT SALMO GAIRDNERI

bу

Kenneth A. Pratt

A THESIS

Submitted to
Michigan State University
in partial fulfillment of the requirements
for the degree of

MASTER OF SCIENCE

Department of Physiology

1982

ABSTRACT

POLAROGRAPHIC DETERMINATION OF THE NORMAL INTRARETINAL OXYGEN TENSION OF THE RAINBOW TROUT SALMO GAIRDNERI

by

Kenneth A. Pratt

The freshwater teleost Salmo gairdneri is capable of concentrating choroidal P_{0_2} to levels 10 times that of the arterial blood, yet the retina of this species shows resistance to the toxicity associated with hyperoxic and hyperbaric oxygen exposure.

Oxygen delivery to the retina of Salmo gairdneri was investigated by measuring the intraretinal P_{0} distribution with polarographic oxygen microelectrodes. The oxygen microelectrodes constructed for this study were advanced through the retina and choroid in 10 μ steps each 15 s while continuously measuring tissue P_{0} .

Results showed that all cell layers of the trout retina are normally exposed to oxygen levels comparable to those known to cause toxicity in other species. Mean retinal P_{0} ranged from 113 to 394 mmHg and increased as the choriocapillaris was approached. Analysis of the P_{0} profile yielded a value of 6.70×10^{-6} ml $0_{2}/\mathrm{min}$ cm atm for the Krogh permeation coefficient at 90.

To my grandparents, Daniel and Lydia Pulter; and to my parents, Richard and Isabell Pratt

ACKNOWLEDGEMENTS

It is a pleasure to acknowledge the guidance, patience, support, and friendship of my major advisor, Jack R. Hoffert, without whose assistance this study would have been impossible.

I also wish to thank the other members of my guidance committee, Drs. William L. Frantz and P.O. Fromm for their critical review of this thesis, and helpful suggestions for its improvement; and Dr. Lester Wolterink for his advice and encouragement during the course of this investigation.

Special recognition and thanks go to Esther Brenke, for the countless hours spent aiding in the construction of P_{0} microelectrodes, and countless more spent typing the rough drafts of this thesis.

Finally, in addition to Dr. Hoffert and Esther, I would like to thank the other members and friends of the Fish Lab: Paul Desrochers, Bill Kreft, Hamdan Noor, Ellen Hanson-Danis, Craig Hartman, and Reuben Stein for the lasting friendships that have been established throughout the course of my graduate study.

I am indebted to the National Eye Institute for the financial support of this project (EY-00009).

TABLE OF CONTENTS

<u> </u>	age
LIST OF TABLESv	rii
LIST OF FIGURESv	riii
INTRODUCTION	1
LITERATURE REVIEW	4
Choroidal Vasculature	4
Mechanism of Countercurrent Multiplication of Oxygen in Swimbladder and Choroidal Retia	8
Oxygen Toxicity	10
Resistance of the Ocular Tissues of the Trout to O ₂ Toxicity	15
Polarographic Oxygen Electrodes	16
Use of Polarographic Oxygen Electrodes in Tissue Oxygen Studies	20
Oxygen Microelectrode Studies on Ocular Tissues	23
Cornea	23
Retina	23
Oxygen Microelectrode Studies on Teleost Retinas	25
MATERIALS AND METHODS	28
Animals	28
Oxygen Microelectrode Construction	28
Anode Construction	30
Characterization of the Pop Microelectrodes	30
Current vs. Salinity	30
Current vs. P ₀₂	31

	Current vs. Temperature	31
	Current vs. Density	31
	Electrode Response Time	32
	Electrode Stability	32
	Microdrive Calibration	32
	Electrode Calibration	33
	Experimental Set-Up	33
	In Vivo Ocular P _O Profile Determination	34
	Localization of Oxygen Profile	34
	In Vitro Ocular P _{O2} Profiles	37
	Data Reduction	
	Determination of Ocular Tissue Thicknesses	38
RES	ULTS	40
	Characterization of the P _{O₂} Electrodes	40
	Electrode Response Time	
	Current vs. Po	40
	Current vs. Temperature	
	Current vs. Salinity	49
	Electrode Stability	49
	Current vs. Density	49
	Ocular Tissue Thicknesses	49
	Retina	49
	Choroid	56
	In Vivo Ocular P _{O2} Profiles	56
	In Vitro Ocular P ₀₂ Profiles	62
DIS	CUSSION	
	P ₀₂ Microelectrodes	64

In Vivo Ocular Poprofiles	65
Retinal P ₀ Profiles	67
In Vivo Profiles	67
In Vitro Profiles	72
Analysis of the Retinal P_{0} Profile	73
SUMMARY AND CONCLUSIONS	84
RECOMMENDATIONS	85
Barriers to Oxygen Diffusion	85
Role of the Falciform Process in Retinal Oxygenation	89
LITERATURE CITED	91
APPENDIX I: Composition of Buffered Ringers Solution	96
APPENDIX II. Calculation of the Kroch Permention Coefficient	07

LIST OF TABLES

TABLE		Page
1.	Ocular tissue thicknesses	59
2.	In vitro retinal P ₀₂ profile	63
3.	Comparison of the measured and predicted retinal P_{0_2} profiles	79

LIST OF FIGURES

FIGUE	R.E.	Page
1.	Diagram of ocular blood flow in the rainbow trout	. 7
2.	Mechanism of countercurrent multiplication of oxygen	. 12
3.	Current-voltage polarogram	. 18
4.	Experimental set-up for the determination of ocular Poprofiles in vivo	. 36
5•	Oxygen microelectrode composition and dimensions	. 42
6.	Electrode response time	. 44
7.	Effect of medium Pop on electrode current	. 46
8.	Effect of medium temperature on electrode current	
9.	Effect of medium salinity on electrode current	- 51
10.	Effect of medium density on electrode curent	• 53
11.	Mean thicknesses of retinal cell layers	• 55
12.	Diagram of possible axes of electrode penetration	. 58
13.	Representative in vivo ocular P _{O2} profile	. 61
14.	Representative in vivo ocular P ₀ profile with diagram of corresponding ocular tissues2	
15.	Retinal P ₀ profile	- 71
16.	Comparison of in vivo and in vitro retinal Pop profiles	
17.	Plot of ln(P ₀₂) vs. electrode position in the retina	. 77
18.	Plot of transformed data for the determination of the Krogh permeation coefficient	. 82
19.	Anatomic arrangement of the swimbladder and choroidal retia of the teleost	. 87

INTRODUCTION

Exposure of animal tissues to oxygen tensions (P_{0_2}) in excess of that found in air may cause both structural damage and cellular dysfunction. Although such toxicity has been documented in a wide variety of species and tissues, the vertebrate eye is unusually vulnerable to the deleterious effects of oxygen, and has received much attention from researchers concerned with the mechanism of oxygen toxicity and means of protection against it. The compelling reason for much of this attention was the discovery in the 1950's that oxygen administration was the cause of retrolental fibroplasia, a vascular disorder that blinded thousands of premature infants. Subsequent studies have shown that a number of other vertebrate ocular tissues, including the retina and choriocapillaris, are susceptible to oxidative damage when exposed to elevated P_{0_2} .

In light of these studies, it seemed incredible when the Wittenbergs, in 1961, reported that the choroidal rete mirabile of most teleosts is capable of concentrating oxygen to levels far in excess of those found in the arterial blood. Several investigators, noting the work of the Wittenbergs, recognized the potential of the teleost as an animal model for the study of ocular oxygen toxicity, and studies were undertaken to determine both the mechanism of oxygen concentration in the choroid and the nature of oxygen delivery to the retinas of these fish. Fairbanks, Hoffert and Fromm (1974) proposed a

mechanism by which the choroid rete mirabile of Salmo gairdneri functions to elevate ocular P_{0} . Their work was based primarily on the findings of Kuhn et al. (1963) who had proposed a similar mechanism for concentration of oxygen in the physoclistous swimbladder of certain teleosts. Fairbanks, Hoffert and Fromm (1969) measured the oxygen tension in the choroidal layer of Salmo gairdneri and found it to be over 400 mmHg. Measurement of the P_{0} in the vitreous body showed it to be much lower, on the order of 100 mmHg, indicating the existance of a large P_{0} gradient within the retina of this species. Precise determination of the intraretinal P_{0} gradient was not accomplished by Fairbanks et al. (1969) probably due to the rudimentary nature of the oxygen electrodes in use at the time of their study.

Although oxygen microelectrode design has been greatly refined in recent years, only Drujan, Svaetichin and Negishi (1971) and Negishi et al. (1975) have reported on the P_{0} distribution in retinas isolated from teleosts, and there are no reports detailing the P_{0} distribution in the retinas of intact fish.

The purposes of the present study were to:

1. Devise a technique for the determination of the intraretinal P_{0_2} distribution in the teleost <u>Salmo gairdneri</u>, in vivo. This will require the construction of reliable oxygen microelectrodes which exhibit rapid, linear response over the wide range of P_{0_2} expected to be encountered in the eyes of these fish.

- 2. Mathematically characterize the intraretinal P_{0_2} gradient and determine values for the parameters governing diffusion of oxygen through the retina (i.e., the Krogh permeation coefficient, oxygen consumption etc.).
- 3. Determine which areas of the retina of Salmo gairdneri are normally exposed to oxygen tensions that would be expected to be toxic to the retinas of other species.

LITERATURE REVIEW

Choroidal Vasculature

Albers in 1806 was the first to show that the horseshoe-shaped body (the choroid gland) found in the choroidal layer of most teleosts, was neither a muscle, nor a secretory gland, as was currently supposed, but was actually a collection of small blood vessels - a form of rete mirabile (Barnett, 1951). Since that time, a variety of functions have been hypothesized for this "wonderful net", (Barnett, 1951) including:

- 1. the choroidal gland is an erectile organ, and acts to expand and push forward the retina, thereby helping to focus images;
- 2. the choroidal gland acts as an agent to dampen pulsations caused by blood flow in arterioles adjacent to the retina;
- 3. the choroidal gland acts as a reservoir for blood supplying the eye; and
- 4. the choroidal gland acts as an organ of biochemical exchange, presumably preventing the loss of some essential substance from the choroidal vasculature to the general circulation.

Barnett (1951) categorically dismissed the first three hypotheses, believing that the unique vascular pattern found in the rete, was indeed well-suited for some type of biochemical interchange. He speculated that the essential substance being retained in the choroidal layer was cytochrome c. Wittenberg and Wittenberg (1961), noting the anatomic similarity between choroidal retia and the retia mirabilia responsible

for transporting high pressures of oxygen into the swimbladders of teleosts, demonstrated that the choroidal rete functioned to build up a large tension of oxygen behind the relatively avascular teleost retina.

The choroidal vasculature has been described in detail, for a number of different species, including: Salmo gairdneri (Copeland and Brown, 1976), Fundulus grandis (Copeland, 1974a and b), Cadus morrhua, Exox lucius, Salmo irideus (Barnett, 1951) and others. Barnett gives a most detailed account of the vascular anatomy of the choroidal gland of the rainbow trout, Salmo irideus. A common vascular pattern, with minor species variations, occurs in all teleosts, and is diagrammed in Blood from the first efferent gill artery supplies the pseudobranch, the remnant of the 1st gill arch in teleosts. passing through the capillaries of the pseudobranch, the blood exits into the ophthalmic artery. The ophthalmic artery passes through the sclera along the optic nerve and branches into an arterial manifold which describes the central margins of the horseshoe-shaped rete. arterial manifold lies within the lumen of a venous sinusoid, and bifurcates almost immediately into the parallel afferent (with respect to the choriocapillaris) capillaries of the rete mirabile. vessels then converge into "distribution" vessels which supply the Blood from the choriocapillaris is drained into choriocapillaris. "collection" vessels which give rise to the efferent capillaries of the The efferent capillaries run parallel to and are interspersed among the afferent capillaries. Blood flow is therefore "countercurrent" within the capillaries of the rete. Blood from the efferent capillaries is collected in the venous sinusoid, and exits the eye in the ophthalmic vein.

Figure 1. Diagram of ocular blood flow in the

rainbow trout. Arrows indicate

direction of blood flow.

RET. - Retina

C.R.M. - Choroidal rete mirabile

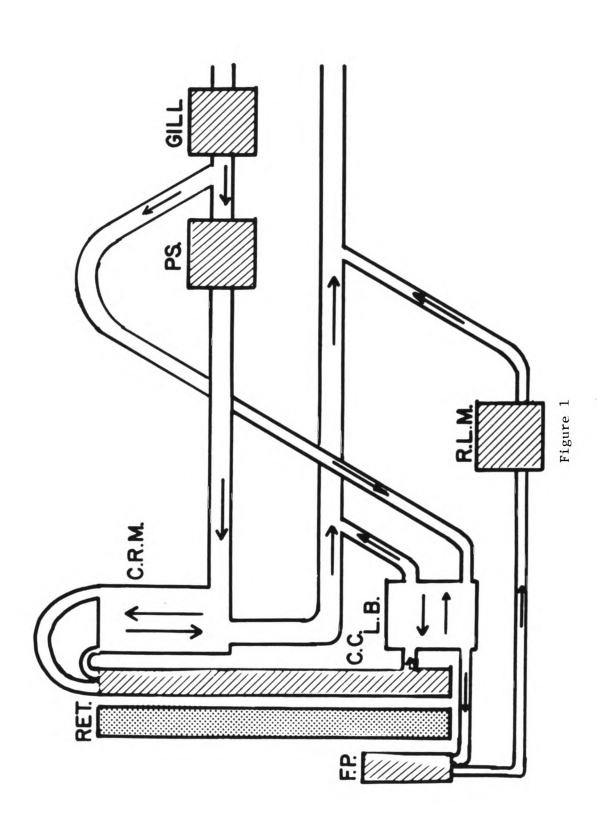
PS. - Pseudobranch

F.P. - Falciform process

C.C. - Choriocapillaris

L.B. - Lentiform body

R.L.M. - Retractor lentis muscle



Mechanism of Countercurrent Multiplication of Oxygen in Swimbladder and Choroidal Retia

The mechanism of oxygen concentration in both the swimbladder and the choroidal rete is believed to be similar (Fairbanks, 1970). Haldane (1922) was the first to suggest that oxygen concentration in the swimbladder rete results from countercurrent multiplication of a primary 0, gradient, formed by addition of acid to the efferent side of the Kuhn et al. (1963), expanded upon this idea, and formulated a detailed hypothesis for the mechanism of 0, concentration. collected from the afferent capillaries of the rete is delivered to a secondary capillary bed (the gas gland; analogous to the choriocapillaris in the eye) which lies adjacent to metabolically active tissue (the secretory epithelium; analogous to the retina) Carbon dioxide is added to the blood, resulting in an increase in the P_{0_2} of the blood entering the efferent capillaries of the rete, by a combination of the Bohr shift and Root shift (decreased binding capacity of Hb for 0_2). The increase in P_{0_2} caused by this "single concentrating effect" drives diffusion of 0, from the efferent to the afferent capillaries in the respective retia. The 02-enriched afferent blood then traverses the connecting capillary bed again, where the entire process is repeated. Repetition of this cycle results in the generation of high levels of oxygen in both swimbladders and choroidal layers of the teleost eye. Maximum efficiency of countercurrent oxygen multiplication is achieved only if the "single concentrating effect" occurs at the correct place, i.e., within the capillary bed between the two sides of the rete. If the unloading of 0, from hemoglobin occurred as blood entered the efferent capillaries, then the available time for

diffusion would be decreased. Berg and Steen (1968) provided evidence that the "Root-off shift" (decrease in plasma pH and subsequent unloading of Hb) has a normal biologic half-time of 0.05 s at 23C, implying that under normal conditions the single concentrating effect probably occurs exclusively within the choriocapillaris and the gas gland capillaries. Acetazolamide, a carbonic anhydrase inhibitor, was shown to abolish the concentration of oxygen in both swimbladders (Fange, 1953) and eyes (Fairbanks et al., 1969) and was thought to act by increasing the $t_{1/2}$ of the Root-off shift from 0.05 s to >30 s (Foster and Steen, 1969). Fairbanks et al. (1969), expanding upon the work of Maetz (1953), arrived at a different explanation for the effect of acetazolamide. They reasoned that carbonic anhydrase, which has been found associated with all tissues connected with countercurrent multiplication of oxygen in choroidal retia, including the pseudobranch, prevents both concentration of CO2 in the eye and "short-circuiting" of the 0_2 multiplication mechanism, by prohibiting the diffusion of ${\rm CO}_2$ from the efferent to the afferent side of the rete. Inhibition of carbonic anhydrase by acetazolamide would presumably result in equilibration of CO2 across the afferent-efferent partition, premature unloading of Hb (increasing the afferent capillary P_{0_2}), abolishment of the P_{0_2} gradient driving diffusion of 0_2 from efferent to afferent capillaries, and a loss of 0, to the general circulation. pseudobranchectomy resulted in a decrease in oxygen concentration in the swimbladders (Copeland, 1951) and the eyes (Fairbanks, 1969) of some fishes, it was concluded that the pseudobranch acted as a source of some of the carbonic anhydrase responsible for maintenance of rete function. A diagramatic summary of the mechanism of 0_2 concentration as proposed by Fairbanks et al. (1974) is given in Figure 2.

A secondary countercurrent system (Figure 1) exists within the eye of most teleosts, and has been described in detail for the rainbow trout, Salmo gairdneri (Copeland and Brown, 1976 and Copeland, 1980). The retinal artery, which arises from the internal carotid and bypasses the pseudobranch, branches into a system of parallel afferent capillaries that lie within the lentiform body. The lentiform body is a small rete mirabile that lies between the limbs of the choroidal rete, ventral to the optic nerve. Blood from the central part of the choriocapillaris drains into a system of efferent lentiform capillaries that interdigitate among the afferent capillaries. The lentiform body therefore acts as a countercurrent exchanger of oxygen. As blood with P_{0} from the choriocapillaris passes through the efferent capillaries of the lentiform body, oxygen diffuses across to the afferent lentiform body capillaries. The efferent capillaries unite into the ventral choroidal vein and blood exits the eye in the ophthalmic vein. The afferent capillaries coalesce into the falciform artery which supplies the highly vascularized falciform process. falciform process is an inversion of the choroidal layer into the vitreous body, through the embryonic fissure of the retina. The falciform process is therefore supplied with oxygen enriched blood from There is no multiplication of oxygen within the the lentiform body. lentiform body, since blood in the afferent lentiform capillaries does not enter the choriocapillaris.

Oxygen Toxicity

Exposure of animals to oxygen tensions (P_0) in excess of those found in air may result in profound deleterious effects, such as cardiac

Figure 2. Mechanism of countercurrent multiplication of oxygen. (A) Retina. Aerobic metabolism results in production of lactate and CO2. (B) Choriocapillaris containing red blood cell. Acidification of blood results in increased P_{0} via Bohr and Root shifts (single concentrating effect). (C) Afferent capillary of choroidal rete. Endothelial wall separating efferent and afferent retial capillaries. (E) Efferent retial capillary. Diffusion of oxygen occurs down its partial pressure gradient from the efferent to the afferent capillaries. Return of blood to the choriocapillaris results in further increase in Po. Repetition of this cycle conserves and concentrates oxygen within the choroidal layer. CO2 is rapidly hydrated in the efferent capillary preventing its diffusion into the afferent capillaries which would cause premature release of oxygen from RBC. (From Fairbanks et al. (1974) with permission).

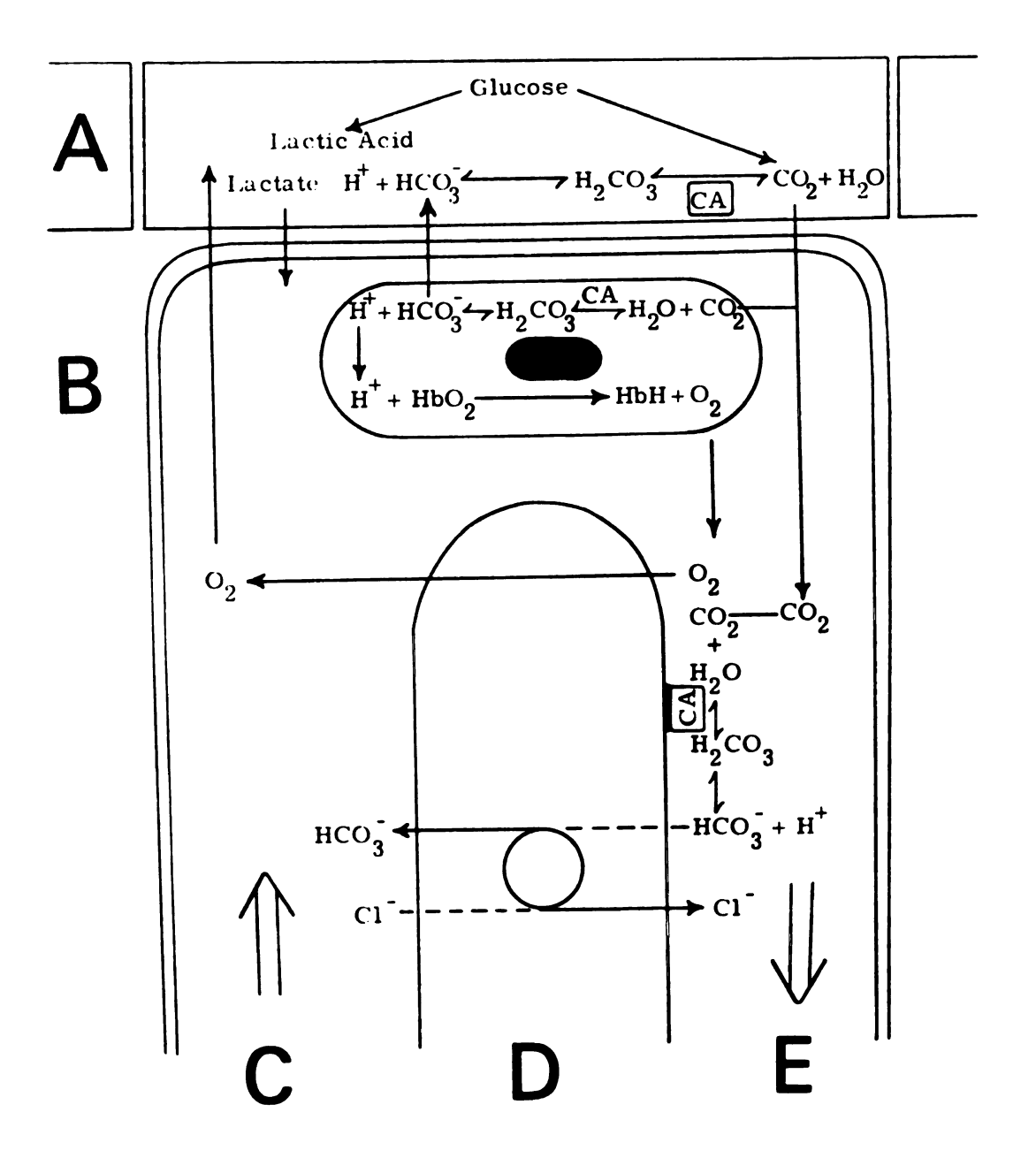


Figure 2

arrythmias, pulmonary lesions, convulsions and death. The toxic effects of oxygen at hyperbaric levels is universal, and has been demonstrated in bacteria, fungi, plants and animals (Fridovich, 1977). Indeed. it appears as if most aerobic organisms exist in a precarious balance between the deadly effects of anoxia, and those of oxygen poisoning. The free radical intermediates of normal metabolic reactions are thought to be the mediators of oxygen toxicity. Excessive production of these free radicals alters metabolism and may cause damage to the structural components of cells. Fortunately, cellular anti-oxidant systems exist which scavenge these oxidating free radicals and immediately render them harmless to the cell. Under conditions of hyperoxia, production of free radicals is thought to increase (Fridovich, 1970). Oxygen toxicity occurs when the anti-oxidant protection systems of the cell become overwhelmed, and cannot keep pace with free radical production. Further review of the theory of oxygen toxicity is provided by Frank and Massaro (1980).

The discovery that oxygen administration was the cause of retrolental fibroplasia, prompted a flurry of investigations into the damaging effects of high oxygen on ocular tissues. Retrolental fibroplasia (RLF) is a disorder of the retinal vasculature that appeared in the 1940's and reached epidemic proportions by the next decade. Retrolental fibroplasia occurred exclusively in premature infants, and was characterized by inhibition followed by proliferation of the retinal vasculature, retinal detachment and consequent blindness. The cause of RLF eluded both researchers and clinicians until 1952, when Patz, Hoeck and De La Cruz determined that the high oxygen atmosphere to which these infants were exposed was in some way responsible for the onset of RLF.

Subsequent studies of ocular oxygen toxicity have been primarily, but not exclusively, aimed at determining the effect of high oxygen on the retinal circulation. Ashton, Ward and Serpell (1953) found that exposure of kittens to 60% oxygen at ambient pressure results in an obliteration of the developing retinal vessels essentially identical to that seen in RLF. The effect of oxygen on the retinal vasculature of several species has been reviewed by Ashton (1970) in which he concludes that "destruction of the growing retinal vessels by hyperoxia is a general biological phenomenon."

The toxic effect of oxygen within the eye is not limited to the retinal blood vessels. Yanoff, Miller and Waldhausen (1970) showed that administration of pure oxygen caused choroidal edema and retinal detachment in dogs. Lucas and Trowell (1958) found that rat retinas in tissue culture survived better in an atmosphere of air than in 60% oxygen. A number of other studies detailed the effect of oxygen on the retinal cells themselves. Noell (1962) found that exposure of adult rabbits to hyperbaric levels of oxygen resulted in a widespread destruction of the visual cells and attenuation of the electroretinogram (ERG). The ERG is widely accepted as an index of the functional integrity of the retina. Noell also showed that exposure to 55% oxygen at ambient pressure for 7 days, resulted in similar effects. Attenuation of the ERG and visual cell death by hyperoxia have also been confirmed in the rabbit (Shaw and Leon, 1970; Bresnick, 1970) as well as in frogs and rats (Ubels, Hoffert and Fromm, 1977).

Investigations have also been carried out on the effect of high oxygen on retinal metabolism. Baeyens, Hoffert and Fromm (1973) demonstrated that exposure of dog retinas to hyperbaric oxygen results

in decreased oxygen consumption, presumably by inhibition of some cellular enzyme system. Earlier studies showed that retinal lactate dehydrogenase (LDH) was one enzyme that could be inhibited by high P_{O2} (Baeyens and Hoffert, 1972). Ubels and Hoffert (1981) found a marked decrease in retinal Na⁺-K⁺ ATPase activity in frogs and rats exposed to hyperbaric oxygen, and suggest that this may in part explain the attenuation of the ERG shown by these species. In summary, exposure of several species to both hyperbaric and hyperoxic partial pressures of oxygen, results in damage to the retinal and choroidal vasculature, as well as to the retinal tissue directly.

Resistance of the Ocular Tissues of the Trout to 02 Toxicity

The choroidal layers of selected teleosts are normally exposed to oxygen tensions in excess of 400 mmHg (Wittenberg and Wittenberg, 1961; Fairbanks et al., 1969). Extended exposure to such high oxygen tensions (at the tissue level) is toxic to the choroid and retinas of other species. This prompted researchers in the 1970's to postulate that the ocular tissues of the teleost have evolved some mechanism of protection against oxygen toxicity. Baeyens and Hoffert (1972) showed that lactate dehydrogenase (LDH) from isolated frog retinas was inhibited by exposure to 100% 0_2 at 1 atm, but that teleost retinal LDH was not. The same investigators found that exposure of isolated teleost retinas to hyperbaric oxygen caused an increase in retinal oxygen consumption, while exposure of frog and rat retinas caused no change and decreased oxygen consumption, respectively. They interpreted these results as further indication that the trout retina is resistant to 0, toxicity. Subsequent studies have shown that the electroretinogram and retinal $\mathrm{Na}^+\mathbf{-K}^+$ ATPase are also less susceptible to inhibition by oxygen in trout than in other mammalian species (Ubels, Hoffert and Fromm, 1977; Ubels and Hoffert, 1981).

Polarographic Oxygen Electrodes

Danneel showed, in 1897, that oxygen could be electrolyzed to the hydroxyl ion in an aqueous solution containing two electrodes, according to the following reaction:

$$0_2 + 2H_2O + 2e^- ---> H_2O_2 + 2OH^-$$
 (1)

(Davies and Brink, 1942; Davies, 1962). The current generated by this reaction has been shown to be proportional to both the concentration of dissolved oxygen and to the applied emf (Davies and Brink, 1942; Fatt, The manner in which the electrode current characteristically varies with the emf (at constant 0, concentrations) is shown in Figure 3. At low voltages (less than is required for reduction of oxygen) a slight residue current exists, due to impurity in the solution (Fatt, 1976). When the O₂ reduction potential is reached the electrode current is approximately proportional to the applied potential, and in this region of the curve reduction of oxygen at the cathode surface results in the establishment of an oxygen concentration gradient between the cathode and the surrounding solution. Diffusion of oxygen to the cathode surface however is fast enough that current is limited only by the applied potential. Increasing the emf in this region results in a faster rate of oxygen reduction, which increases the rate of 0_2 diffusion from the surrounding medium. When the applied emf is high enough, the oxygen concentration at the cathode surface approaches zero, as each 02 molecule is immediately reduced to hydroxyl ion. electrode current at this point is now limited only by the rate of

Figure 3. Current-voltage polarogram. This plot shows the characteristic manner in which electrode current varies with the applied voltage. The plateau region of the curve is centered around 0.7 volts. Polarizing voltage is maintained at 0.7 volts during the measurement of tissue P_0 as small changes in voltage will not greatly affect electrode current at this voltage.

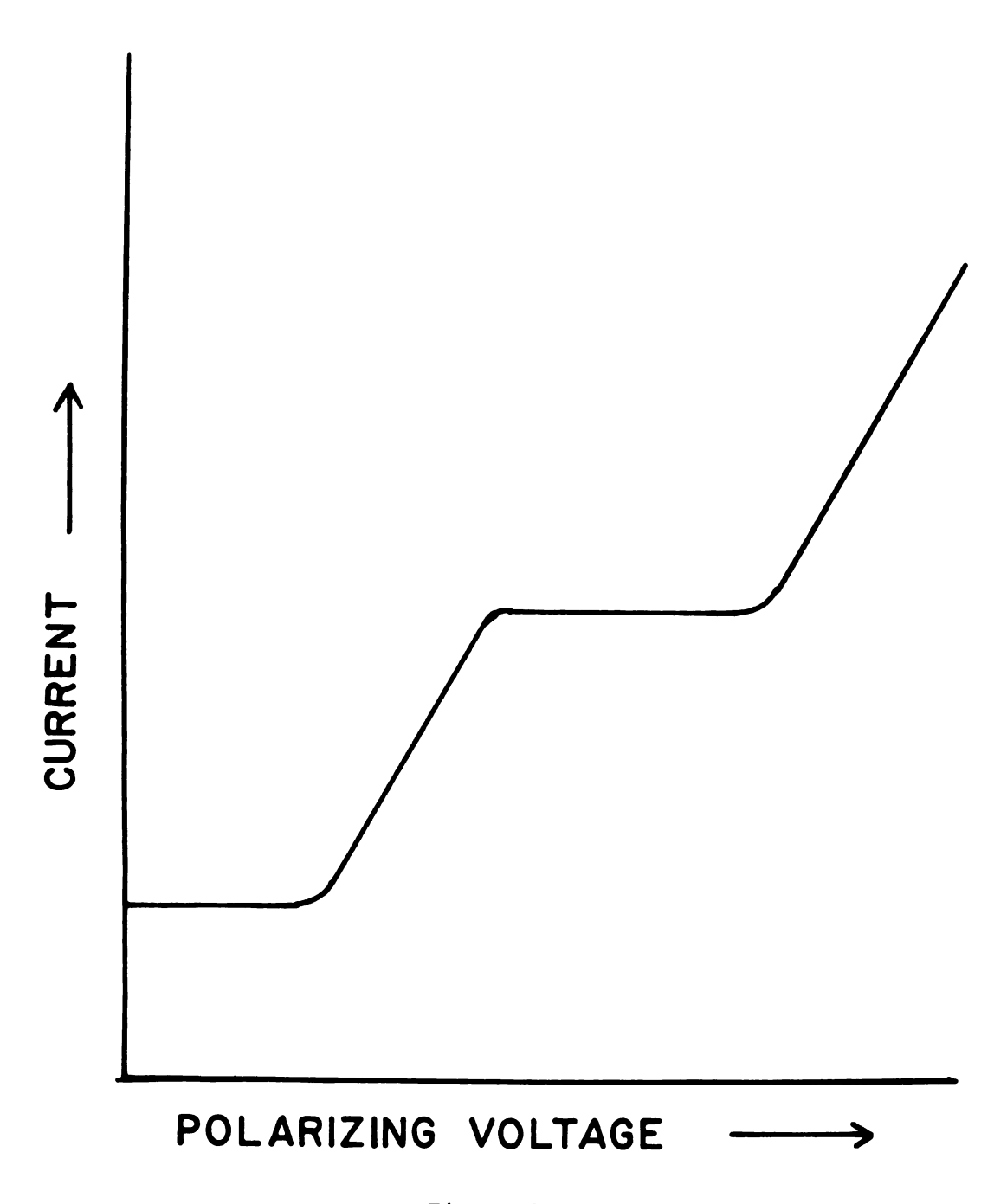


Figure 3

diffusion of oxygen (i.e., the P_{0_2}), and not by the applied emf. This is reflected by the "plateau region" of the current-voltage curve. The plateau region exists between 0.6 and 1.0 volts in the case of oxygen. Increasing the emf past 1.0 volts results in another increase in the current, as a second reaction (reduction of H^+) begins to occur.

Davies and Brink (1942) were the first to use oxygen electrodes for the measurement of P_{0} in living tissue. The electrodes constructed by Davies consisted of a platinum wire cathode, fused within a glass capillary tube which projected slightly beyond the platinum wire. Platinum was used to prevent any side reactions (i.e. reduction of biological tissue components), from interfering with the "oxygen" current. The recessed electrode tip was found to be necessary, in order to determine absolute values for oxygen tensions. The oxygen cathode used in conjunction with a nonpolarizable reference anode. Insulated noble metal cathodes used with nonpolarizable reference anodes are still the oxygen electrodes of choice today. However several modifications of this basic design have evolved in recent years. Schneiderman and Goldstick (1975) showed that the length of the recess should be approximately eight to ten times the diameter of the cathode tip, in order to confine the diffusion gradient within the recess. This insures an accurate measurement of the Poo that exists at the tip of the Recessed electrodes also eliminate the effects of stirring of the medium. Since electrode response time increases with increasing recess length, most P_{0_2} electrodes have been constructed in such a way as to minimize electrode diameter. Whalen et al. (1967) constructed cathodes with tip diameters of 1-2 micrometers and a recess length of 30 micrometers. These electrodes showed response times of less than 1 s.

Both Davies and Brink (1942), and Whalen et al. (1967) found that filling the recess with a membrane that is permeable to oxygen but not to proteins, improves the stability of oxygen electrodes. Clark et al. (1953) designed an electrode which incorporates both cathode and nonpolarizable anode behind a protein impermeable membrane. Fatt (1964) refined the design of the "Clark" electrode by devising a method for constructing electrodes with tip diameters of approximately one micrometer. This provided for spatial resolution of tissue P_{0_2} , comparable to that found in the "Whalen-type" electrode. Nonetheless it is the solid metal cathodes of the type designed by Whalen that have found the most extensive use in biological research.

Use of Polarographic Oxygen Electrodes in Tissue Oxygen Studies

Since their advent, oxygen microelectrodes have proven to be a powerful tool for the study of tissue oxygenation. Ganfield, Whalen and Nair (1970) measured the oxygen tension profile through a slice of cat cortical tissue, and showed that the measured tissue P_0 distribution closely fit the distribution predicted by classical diffusion theory. Hill (1928) showed that one dimensional diffusion of oxygen into a homogeneous sheet of respiring tissue is described by the following equation:

$$dy/dt = D(d^2y/dx^2) - v_{0_2}$$
 (2)

where: y = concentration of 0₂,

t = time,

V₀₂ = oxygen consumption,

x = distance into the tissue sheet,

and D = the diffusion coefficient for 0_2 .

Inherent within this model are the following assumptions: 1) the oxygen supply at x = 0 is constant, 2) oxygen diffuses in the direction of the x axis only, and 3) \dot{v}_{0_2} and D are both constant and independent of P_{0_2} . In the steady state, dy/dt = 0 and equation (2) becomes:

$$0 = D(d^2y/dx^2) - \dot{v}_{0_2}$$
 (3)

The general solution of this equation is:

$$y = \dot{v}_{0_2} x^2 / 2D + Bx + y_0$$
 (4)

where: y_0 = the 0_2 concentration at x = 0. The value B in equation (4) is a constant, to be determined by the boundry conditions of the model. If oxygen is supplied from one source only then a point x' must be reached within the tissue where $y_{x'}$ = 0, at which time diffusional flow must stop. At this point (x'):

$$y = 0 = \dot{v}_{0_2}(x^2)^2/2D + Bx^2 + y_0$$

and $dy/dx = 0 = \dot{v}_{0_2}x^{-}/D + B$ solving for B yields;

$$B = -(2\dot{v}_{0_2} v_0 / D)^{1/2}$$

and the particular solution describing the oxygen distribution as a function of x (for the given boundry conditions) becomes:

$$y = \dot{v}_{0_2} x^2 / 2D - (2\dot{v}_{0_2} y_0 / D)^{1/2} x + y_0$$
 (5)

Using the relationship:

$$P_{0_2} = y / S$$

where P_{0_2} = oxygen tension, y = concentration of 0_2 and S = oxygen solubility coefficient, equation (5) may be rewritten as:

$$P_{0_{2}} = (\dot{v}_{0_{2}}/2DS)x^{2} - (2\dot{v}_{0_{2}}(P_{0_{2}})/DS)^{1/2}x + (P_{0_{2}})$$
 (6)

where $(P_0) = P_0$ at the oxygen source. The product of D and S is the Krogh permeation coefficient.

Ganfield et al.(1970), reasoned that if the above diffusion model holds, then the P_{0_2} distribution measured in their tissue preparation should be described by equation (6). To facilitate the data analysis, they rearrange equation (6) into:

$$[(P_{0_2})_0 - P_{0_2}]/x = (2\dot{V}_{0_2}(P_{0_2})_0/DS)^{1/2} - \dot{V}_{0_2}x/2DS$$
 (7)

If the model holds, then a plot of $[(P_{0_2}) - P_{0_2}]/x$ vs. x should yield a straight line. They find that such a plot of the data does approximate a straight line, in all regions of tissue where $P_{0_2} > 2$ mmHg. Furthermore they were able to calculate values for V_{0_2} and for DS, based upon their data and the above plot. Oxygen consumption was calculated by determining the flux of oxygen into the tissue and the average distance within the tissue where P_{0_2} fell to O. The volume of tissue being supplied by the measured P_{0_2} flux was calculated and oxygen consumption determined. The Krogh permeation coefficient (DS) was determined by measuring the slope of the line of $[(P_{0_2})_0 - P_{0_2}]/x$ vs. x. The slope is equal to $-V_{0_2}/2$ DS (see equation (7)). Thus if V_{0_2} is known, DS may be readily determined from the slope. Ganfield et al. (1970) report an a V_{0_2} value of 0.0898 ml V_{0_2}/x tissue min, and a DS value of 1.29x10⁻⁵ ml V_{0_2}/x min cm atm for cat cerebral cortex.

Oxygen Microelectrode Studies on Ocular Tissues

Cornea

Takahashi and Fatt (1965) devised a method for the empirical determination of the diffusion coefficient of isolated, non-respiring rabbit and bovine corneas. Their experimental set-up consisted of an isolated cornea draped over a Clarke polarographic oxygen electrode within an air tight chamber. The gas filling the chamber was abruptly changed from air to nitrogen, and the time course of the resultant fall in P_{0} at the electrode tip was analyzed for the oxygen diffusion coefficient. They report a D value of 0.667×10^{-5} cm²/s for rabbit corneas at 33C and 0.535×10^{-5} cm²/s for bovine corneas at 4C. Takahashi, Fatt and Goldstick (1966) refined this method and determined both oxygen consumption and the oxygen diffusion coefficient of respiring rabbit corneas. They reported an oxygen consumption value of 0.57×10^{-5} ml $0_{2 \text{ STP}}/\text{ml}$ tissue's and a diffusion coefficient value of 0.5×10^{-5} cm²/s at 25C. Fatt and Bieber (1969) and Fatt (1969) used the values determined for D and V_{0_2} in the previous studies, along with a mathematical analysis similar to that used by Ganfield et al. (1970) to predict the P_{0} distribution through human corneas exposed to air and when covered by a contact lens. These investigators report no attempt to directly measure intracorneal P_{0_2} , presumably because the corneal tissue offers too great a mechanical resistance to electrode penetration.

Retina

Alm and Bill (1972) and Alm (1972) studied the effects of changes in various hematological parameters, and administration of various vasoactive agents, on feline retinal oxygen tension. Rather than measure

the oxygen tension of the retina directly, these investigators measured the P_{0_2} of the vitreous at a point located near the inner limiting membrane. Oxygen microelectrodes, shielded by a cannula inserted through the pars plana were advanced past the lens and into the vitreous body. They suggest that changes in retinal P_{0_2} will be reflected by changes in P_{0_2} at the tip of a microelectrode so situated. In an attempt to locate the position in the retina from which P_{0_2} was estimated, a steel needle was inserted through the cannula vacated by the electrode at the conclusion of each experiment. The needle was pushed into the retina and the eye later removed and opened so that the location of the needle could be noted.

Zuckerman and Weiter (1980a) used macro and micro oxygen electrodes to measure oxygen consumption and the P_{0_2} profile through isolated bullfrog retinas. They found that dark adapted retinas exhibit greater oxygen consumption and an increased P_{0_2} gradient than do light adapted retinas. They attribute these differences to a large ionic current associated with dark adapted photoreceptor cells. They attempt to verify this hypothesis by plotting the first spatial derivative of the intraretinal P_{0_2} profile as a function of position within the retina $(dP_0)/dx$ vs. x). Their plot for dark adapted retinus shows a marked peak at an area corresponding to the photoreceptor inner segments. They conclude that, in the dark, oxygen consumption is highest at the level of the inner segments. Zuckerman and Weiter's interpretation of the plot of dP_0/dx vs. x has come under criticism by Tsacapoulos and Poitry (1980) who favor an analysis similar to that of Ganfield et al. (1970). In rebuttal, Zuckerman and Weiter (1980b) claim that the assumptions of constancy of retinal D, S and V_{02} are not valid in their case, making the analysis of Ganfield et al. (1970) meaningless. Zuckerman and Weiter further argue that the absence of the peak in a plot of dP_0 /dx vs. x for the data obtained from light adapted retinas lends support for concluding that a high oxygen consumption is associated with the photoreceptor dark current. It should also be reported that Santamaria et al. (1971) found no difference in oxygen consumption in light adapted versus dark adapted teleost retinas.

Tsacopoulos, Poitry and Borsellino (1981) measured the oxygen consumption and P_{0_2} profile through isolated honeybee drone (Apis mellifera) retinas. Using an analysis identical to that of Ganfield et al. (1970) they calculate and report values for the parameters governing oxygen delivery to the retinas of these drones. The values reported by Tsacopoulos et al. (1981) are: $v_{0_2} = 18 \,\mu\text{l}\,\,0_2/\text{cm}^3$ tissue min; D = $1.03 \,\text{x}\,10^{-5}$ cm²/s and S = $54 \,\mu\text{l}\,\,0_2 \,\text{STP}/\text{cm}^3$ atm, all calculated from data obtained at 22C. They further conclude that only a small fraction of the oxygen consumption of dark adapted drone retinas is required for maintenance of the sodium pump, i.e., the magnitude of the dark current is small in this species.

Oxygen Microelectrode Studies on Teleost Retinas

Interest in oxygen delivery to the teleost retina resulted primarily from the pioneering studies done by Wittenberg and Wittenberg in the early 1960's. Their prediction and subsequent verification of the high oxygen concentrations found in teleost eyes initiated a series of studies of the unique nature of oxygen delivery to the retinas of these fish. Wittenberg and Wittenberg (1962) using relatively large oxygen electrodes, measured the P_0 in the eyes of a number of marine teleosts, and found a direct correlation between the measured oxygen tension and

the degree of choroidal rete development. The electrode was inserted through the cornea toward the retina, to a point in the vitreous body believed to be immediately in front of the retina. They report a range of vitreous body oxygen tensions from 19 mmHg, (in those fish with poorly developed retia), to 775 mmHg, (in fish with highly developed retia). Fairbanks (1968) and Fairbanks et al. (1969) used a similar method to measure the oxygen tension immediately behind the retina, as well as in the vitreous body of the freshwater teleost, Salmo gairdneri. They too found oxygen tensions greatly in excess of the animal's arterial blood P_{0_2} . Fairbanks et al. (1969) report a mean "retinal" P_{0_2} of 445 mmHg and a mean vitreous body P_{0_2} of 103 mmHg for Salmo gairdneri. They suggest that the large difference between the P_{0_2} in back of the retina and the P_{0_2} in the vitreous chamber is due to oxygen consumption by the avascular retina.

Negishi et al. (1975) were among the first to measure and report the P_{0_2} profiles through retinas isolated from vertebrate eyes. Their studies were done on two teleost species, <u>Eugerres plumieri</u> and <u>Centropomus undecimalis</u>. They found that when a platinum oxygen microelectrode was advanced through the retinas of these fish in steps of 25 μ , the P_{0_2} decreased stepwise, with the largest reductions in P_{0_2} occurring at the level of the photoreceptors. They interpret this observation as implying a higher rate of oxygen consumption at the photoreceptor layer. They also found that if the P_{0_2} of the receptor cell layer is maintained at 128 mmHg the oxygen tension at the innermost layers of the retina approaches zero. This result is compatible with the findings of Fonner, Hoffert and Fromm (1973) who noted that trout electroretinograms begin to indicate an hypoxic condition when

photoreceptor P_{0} falls below 100 mmHg. Negishi et al. (1975) also reported observations on the P_{0} levels in the retina in situ. They state that "oxygen was found to distribute through all retinal layers at a high oxygen tension of about 20 per cent (128 mmHg) or more", and that "a marked P_{0} gradient was found, increasing from vitreal surface to choroid." Unfortunately, the method used for determining the intraretinal profiles in situ was not detailed.

MATERIALS AND METHODS

Animals

All experiments were performed on rainbow trout, <u>Salmo gairdneri</u>. The fish were obtained from Midwest Fish Farming Enterprises in Harrison, MI and were transported to E. Lansing in insulated steel tanks equipped with aeration devices. The fish were then housed in fiberglass tanks through which aerated, dechlorinated tap water continuously flowed. Temperature was maintained at 9±1C and photoperiod was 16L:8D. The trout were fed commercial trout chow (Ralston Purina Co., St. Louis, MO) 1-2 times weekly. All fish used in these studies weighed between 150 and 300 g.

Oxygen Microelectrode Construction

Electrodes were constructed according to the method of Whalen et al. (1967) with minor modifications. Five microliter (5µl) glass pipettes (Corning, #70995) were preheated on a clean, electrical hot plate at 2000 overnight. The pipettes were then filled approximately 2/3 the length with molten Wood's metal (Baker Chemical Co., Phillipsburg, NJ) using an oiled syringe and appropriate size polyethylene tubing. The filled tubes were placed in a muffle furnace, preheated to 2000, and allowed to slowly cool to room temperature by turning the furnace off. This process was usually accomplished overnight. The capillary tubes were then placed in a microelectrode puller (Industrial Science Assoc., Inc., Model #M1), such that the platinum heating coil was positioned

around the end of the tube containing no Wood's metal. Temperature controls on the microelectrode puller were adjusted such that the resulting electrode had a smooth taper to a relatively small tip (0.d.~10 μ). The electrode was then returned to the hot plate (2000), and a piece of copper wire was inserted into the lumen of the tube at the end opposite to the tip. The Wood's metal column was teased down into the tip of the electrode, by alternatingly heating and cooling the tip, and by using the copper wire as a plunger. The resulting electrode consisted of a micropipette with small tip, completely filled with Wood's metal. The copper wire was left in place as an electrical connector. A small recess was formed in the tip by electrically etching the Wood's metal column back the desired length. This was accomplished by applying 25-30 V (DC) to the electrode (anode), the tip of which was submerged in gold plating solution (Hoover and Strong, NY,NY) along with a pure gold foil cathode. This process was viewed with the aid of a compound microscope at low power. Best results were often obtained when the voltage was intermittently interrupted, and when polarity was intermittently reversed. Recess length was usually set at approximately 50 μ , and was always at least 8-10X the i.d. (~5 μ). Using the same set-up, a 1-5 µ layer of pure gold was then electroplated onto the tip of the Wood's metal column. Plating voltage was ~1.0 V and the electrode was attached as a cathode (pure gold foil anode). plating and time necessary for obtaining the desired recess length were The recessed electrode was then washed overnight in both variable. distilled water to remove the plating solution. Finally, the tip recess was filled with a protein impermeable membrane, either 50% collodion (Baker Chemical Co., Phillipsburg, NJ), 50% ether v/v; or 50% Rhoplex (Rohm and Haas Co., Philadelphia, PA), 50% water v/v, by submerging the tip in the appropriate solution for approximately 10 min. Best results were obtained with Rhoplex.

Anode Construction

Anodes were constructed as follows: 20 gauge silver wire (Sargent Scientific Laboratory Supplies, Detroit, MI) was cleaned with fine emery cloth and washed with distilled water. A 3-5 cm piece of wire was attached to an AC voltage source and submerged in a plating solution consisting of 0.1 N HCl. A second piece of silver wire was similarly submerged as the second electrode. The electrodes were plated at 6.3 volts for the length of time required for them to turn uniformly purple in color (~5 min). The finished anodes were stored in 0.9% NaCl solution in the dark until needed.

Characterization of the Po2 Microelectrodes

Current vs. Salinity

The effect of changes in medium salinity on electrode current were determined by exposing the cathode to four saline solutions, at constant temperature and P₀, but varying concentrations of NaCl. The solutions contained 83, 164, 249, and 332 mM NaCl respectively. The electrode was allowed to equilibrate in each solution, after which time ten current determinations were made, over a period of 3-5 min and a mean current value calculated. Current was amplified and displayed on a chemical microsensor (Transidyne General Corp., Ann Arbor, MI, Model 1201). The data were then plotted as current vs. NaCl concentration, and the slope of the regression line was tested for significance.

Current vs. Po

The linearity of electrode response as a function of increasing P_{0_2} was tested by exposing the cathode to solutions at constant temperature and salinity, but varying P_{0_2} 's. The solutions consisted of 154 mM NaCl at room temperature, through which pure oxygen, pure nitrogen and air respectively were bubbled. Complete saturation of each solution was assumed, i.e., the P_{0_2} 's were 741, 0 and 155 mmHg for P_{0_2} and air respectively. After allowing approximately 30 seconds for equilibration in each solution, 10 current readings were made and averaged. The data were then plotted as electrode current vs. medium P_{0_2} and tested by regression analysis.

Current vs. Temperature

The effect of medium temperature on electrode current was tested by exposing the oxygen cathodes to solutions at constant salinity (154 mM NaCl) and P_{02} (~155 mmHg), but varying temperatures. Three solutions were maintained at 10C, 23C, and 37C respectively. After allowing ~30 s for equilibration in each solution, 10 current measurements were made, and mean values determined. The data were then plotted as electrode current vs. medium temperature and the slope of the regression line analyzed.

Current vs. Density

The effect of medium density on electrode current was tested by advancing the electrode through agar gels of varying density at constant P_{02} and temperature. Non-nutrient agar (Difco Laboratories, Detroit, MI) was prepared in sterile saline at concentrations of 2.5, 5.0, 7.5 and 10.0 g/dl. A cube of agar was formed in such a way that it contained four layers, each approximately 2mm thick and containing agar of

different density. This agar cube was allowed to stand for 24 h in room air to ensure an equilibration of P_{0} throughout. The cube was then submerged in air saturated saline, and an oxygen microelectrode advanced through each layer while current was measured and recorded.

Electrode Response Time

The response time of the oxygen microelectrodes was determined by abruptly changing the P_0 of the external medium. This was accomplished in the calibration chamber, by allowing the electrode to equilibrate in an air saturated saline solution and then abruptly injecting an 0_2 saturated saline solution. The time course of the increase in electrode current was recorded on a strip-chart recorder, set at high speed (1 inch/s). The time required to reach 90% of the full response was determined.

Electrode Stability

The stability of the electrode current was tested by placing an electrode in a 154 mM NaCl solution through which either pure $\mathbf{0}_2$ or air was continuously bubbled. Electrode current was then continuously measured and recorded for a period of 2 h, and the percent variation in current calculated.

Microdrive Calibration

Prior to any ocular Pop determinations, the hydraulic microdrive (Frederick Haer and Co., Brunswick, MA, Model 50-11-4) was calibrated by measuring the distance the electrode moved while the microdrive was in operation, and determining an appropriate correction factor for the digital readout of the microdrive. This became necessary when it was discovered that the microdrive readout was not a correct measure of the actual distance traveled by the electrode.

Electrode Calibration

The oxygen microelectrode was calibrated in 154 mM NaCl solutions, maintained at constant temperature ($\sim 9\pm 1$ C) through which pure technical grade nitrogen, and pure oxygen respectively were bubbled. If the current in the solution containing nitrogen (0% 0₂) was found to be >10% of the current of that in pure oxygen (100% 0₂) the electrode was discarded and replaced (Whalen, Nair and Ganfield, 1973). The electrode was calibrated before and after each ocular P_{0_2} determination. Data were retained only in experiments where the two calibration readings differed by less than 10%.

Experimental Set-Up

Prior to a P_{0} profile determination, the fish was anesthetized with MS-222 (tricane methane sulfonate; Ayerest Laboratories Inc., NY,NY) to a stage deep enough that the righting reflex was lost. The fish was then paralyzed by intraperitoneal administration of approximately 10 mg of tubocurarine chloride (Eli Lilly Co., Indianapolis, IN). In some cases the fish was also singly pithed to ensure paralysis. While still under anesthesia, the fish was then anchored on its side in a small salinefilled Plexiglass chamber by passing a brass rod through the upper and lower jaws. A catheter was inserted into the buccal cavity, and aerated isotonic saline directed across the gills. Flow rate was maintained at ~500 ml/min, a rate which has been shown adequate to support the electroretinogram (Hoffert and Ubels, 1979). Temperature of the saline bath was maintained at ~9±0.5C and was continuously monitored with a telethermometer (Yellow Springs Instrument Co., Yellow Springs, OH, Model 43TD). A small incision was made in the nasal side of the cornea, and the calibrated oxygen microelectrode, shielded by a 13 gauge hypodermic needle cannula, was inserted through the incision, past the lens and into the vitreous chamber. In several experiments 2% procaine hydrochloride (Mizzy Inc, NY,NY;) was applied topically to the cornea before the incision was made.

The electrode was positioned approximately 2-3 mm anterior to the retina with the aid of a micromanipulator (Pfeiffer Research Instruments; Valley Stream, NY, Model TMX-1). The reference anode was placed in the circulating saline bath outside the animal. The experimental set-up is diagrammed in Figure 4.

In Vivo Ocular Po Profile Determination

All P_{0_2} profile determinations were made under conditions of normal room light. After allowing several minutes for the electrode current to stabilize, the electrode was advanced along the optical axis through the retina and choroid in 10 μ steps every 15 s. Current from the electrode was amplified and displayed as volume percent 0_2 by a chemical microsensor. The polarizing voltage was supplied by the microsensor and was maintained at -0.7 volts in all experiments, as this was the voltage found to be associated with the plateau region of the current-voltage polarogram. Electrode current was also recorded as volume percent 0_2 vs. electrode penetration depth on a strip chart recorder (Moseley Division, Hewlett Packard Co., Pasadena, CA, Model 7100B). The electrode was advanced through the choroidal layer until a precipitous fall in P_{0_2} to a level of approximately 0 mmHg was noted whereupon penetration was stopped.

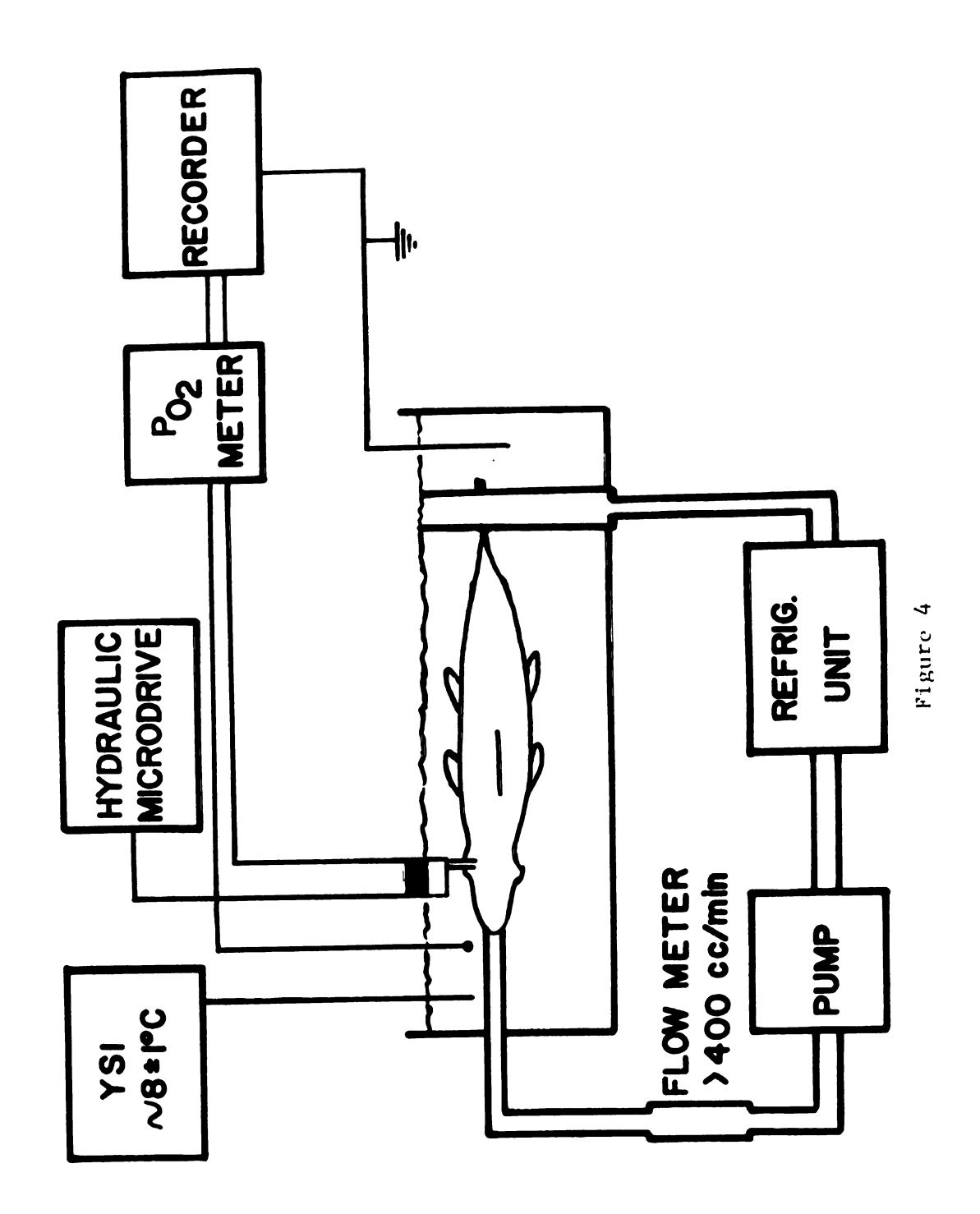
Localization of Oxygen Profile

Following each determination of ocular P_{0_2} , an attempt was made to determine the region of the eye through which the electrode was

the
for
set-up
Experimental
Figure 4.

determination of ocular $^{\mathrm{P}}_{0_2}$

profiles in vivo.



advanced. At the close of each experiment, the oxygen microelectrode was removed from the eye, leaving the hypodermic needle cannula in place. A second, dummy electrode was inserted through the cannula and into the back of the eye until it became lodged in the sclera. care was taken to move neither the fish nor the cannula during this The fish was then removed from the chamber, immediately procedure. killed by decapitation, and the head quickly frozen in dry ice and While still frozen, the eye was removed from the head and prepared for sectioning, so that the position of the marking electrode could be determined. Each eye was placed on a freezing microtome, and transversely sectioned in 50 µ increments, until the marking electrode The electrode axis was determined by noting the ocular was reached. structures through which the electrode passed (i.e., choroidal rete, optic nerve, etc.).

In Vitro Ocular Po Profiles

In order to obtain retinal P_{0_2} profiles in vitro, fish were killed by decapitation and an eye enucleated. A relatively large (~2mm diameter) hole was made in the sclera near the optic nerve. The eye was then placed cornea down in a Plexiglass chamber through which a buffered Ringer solution (Appendix I) was circulated. Pure oxygen was bubbled through the chamber and the temperature of the solution was maintained at ~10±0.5C. The calibrated oxygen microelectrode was positioned over the hole in the sclera and advanced through the choriocapillaris and retina in 10 μ steps while P_{0_2} was continuously monitered and recorded as in the \underline{in} \underline{vivo} P_{0_2} determinations.

Data Reduction

The strip chart recordings of volume percent oxygen vs. electrode penetration depth were converted to plots of P_{0_2} vs. electrode depth with the aid of a computer program and plotting routine. Appropriate corrections were made for ambient barometric pressure. Values of P_{0_2} were calculated for each 1 μ of electrode penetration by interpolating the data between each depth where P_{0_2} was actually measured. The data were also transformed such that plots of dP_{0_2}/dx vs. x, and $[(P_{0_2})_0 - (P_{0_2})_x]/x$ vs. x could be obtained. Computer programs were similarly written to assist in these transformations of the data.

Determination of Ocular Tissue Thicknesses

In order to correlate the measured oxygen tensions to the various ocular tissues through which the electrode passed, it became necessary to determine the cross-sectional thicknesses of the retina, choriocapillaris and other choroidal structures. Several fish were killed by decapitation and quickly frozen in dry ice and ethanol. The eyes were placed on a freezing microtome and transversely sectioned to a point approximately 500 u dorsal to the optic nerve. Color slides were made of the sectioned eye and a reference length marker. The finished slides were then projected, and the mean thickness of each respective ocular tissue determined along several possible axes of electrode penetration. The contribution of each of the retinal cell layers to the total retinal thickness could not be determined by this method, because the cell layers are indistinguishable in frozen section. The absolute thickness of each cell layer was estimated by fixing, preparing and sectioning paraffin embedded eyes, and staining with hemotoxylin and eosin. Although fixation of the tissue results in shrinkage, the percentage contribution of each cell layer to the total retinal thickness can be determined in paraffin sections and related to absolute retinal thickness as measured in frozen section. It was assumed that tissue shrinkage was linear during fixation.

RESULTS

Composition and dimensions of a finished oxygen microelectrode are shown in Figure 5. Results of the tests of electrode response characteristics are outlined below.

Characterization of the Po2 Electrodes

Electrode Response Time

A characteristic plot of electrode current vs. time following an abrupt increase in the P_{0} of the calibration medium is given in Figure 6. For this electrode, 90% of the total response was obtained within 2.5 s. Although not shown in Figure 6, similar results were obtained following an abrupt decrease in the P_{0} of the medium.

Current vs. Po

The linear relationship between electrode current and P_{0_2} is illustrated in Figure 7. This relationship held over a P_{0_2} range of 0 to 741 mmHg, and nearly all tissue P_{0_2} 's measured in trout eyes fell within this range. The coefficient of determination for these data was 0.998.

Current vs. Temperature

Electrode current was also found to vary as a linear function of medium temperature (Figure 8). The coefficient of determination for these data was 0.951. The temperature coefficient was calculated to be 3.63%/C over a range of 10-37C.

Figure 5. Oxygen microelectrode composition and dimensions. Drawing not to scale.

I.D. - Inner diameter

O.D. - Outer diameter

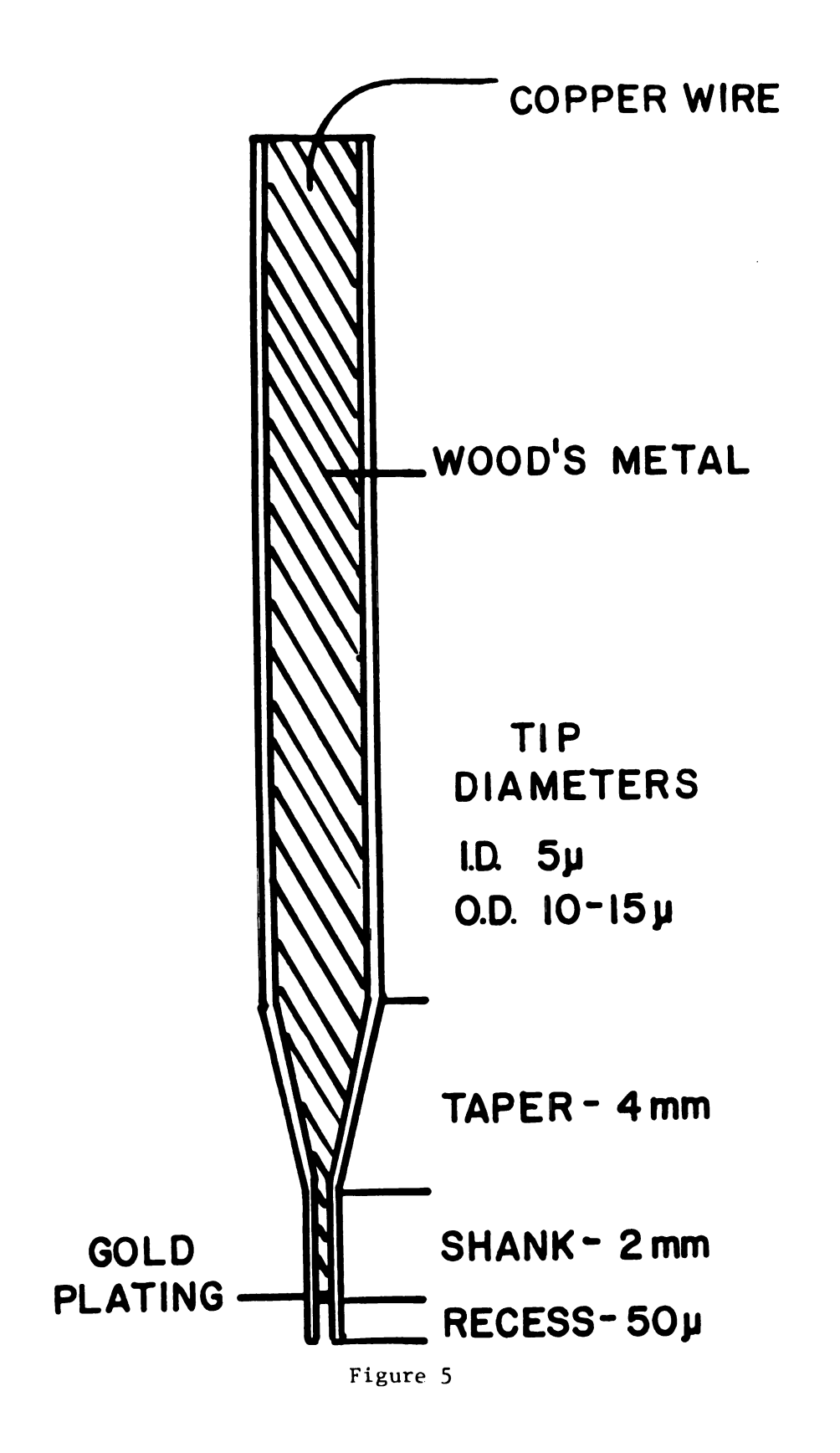


Figure 6. Electrode response time. A plot of

electrode current vs. time, recorded at 22C. P_{0_2} of the calibration medium was abruptly increased at time = 0. Ninety percent of the full response was

obtained within 2.5 seconds.

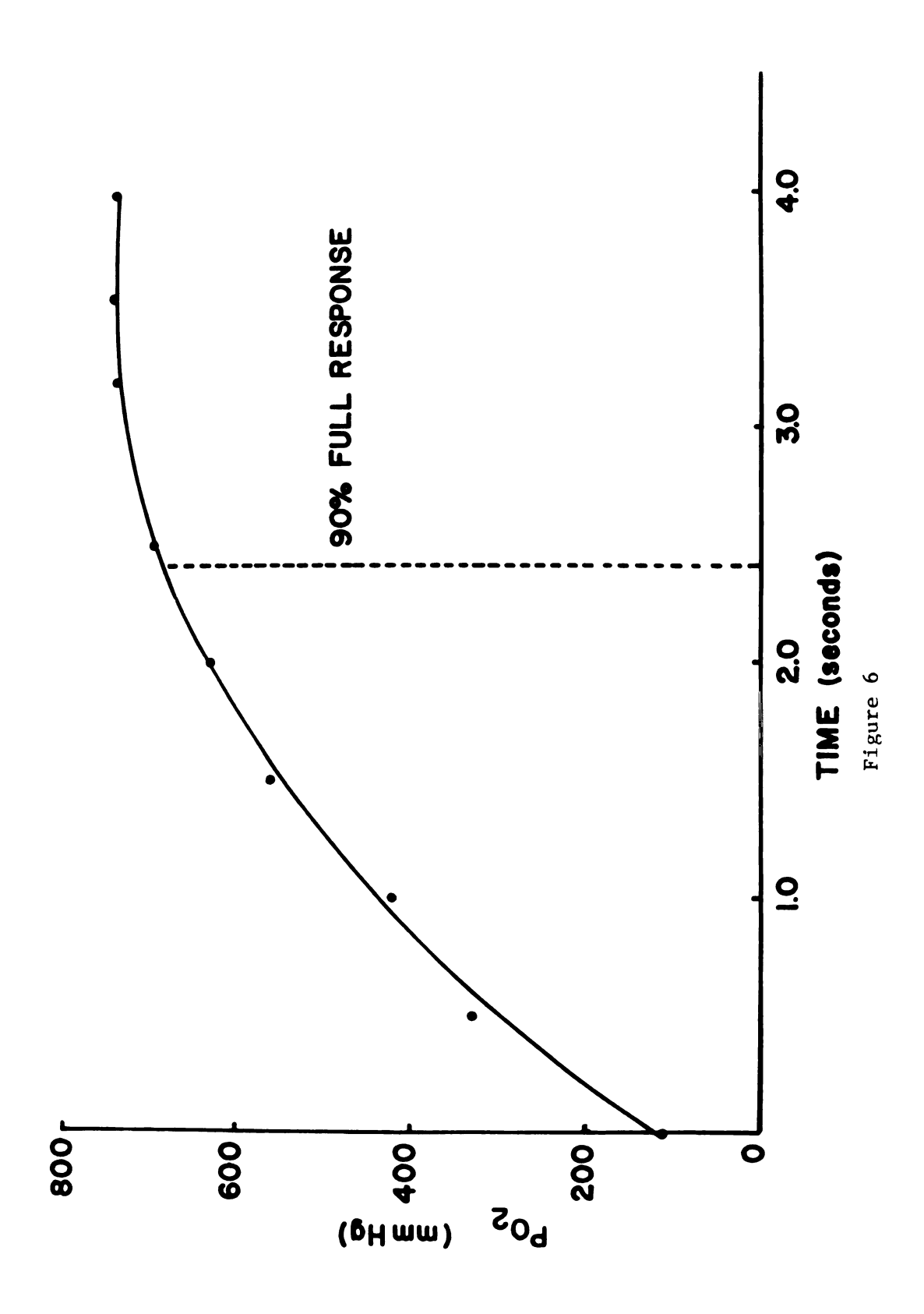
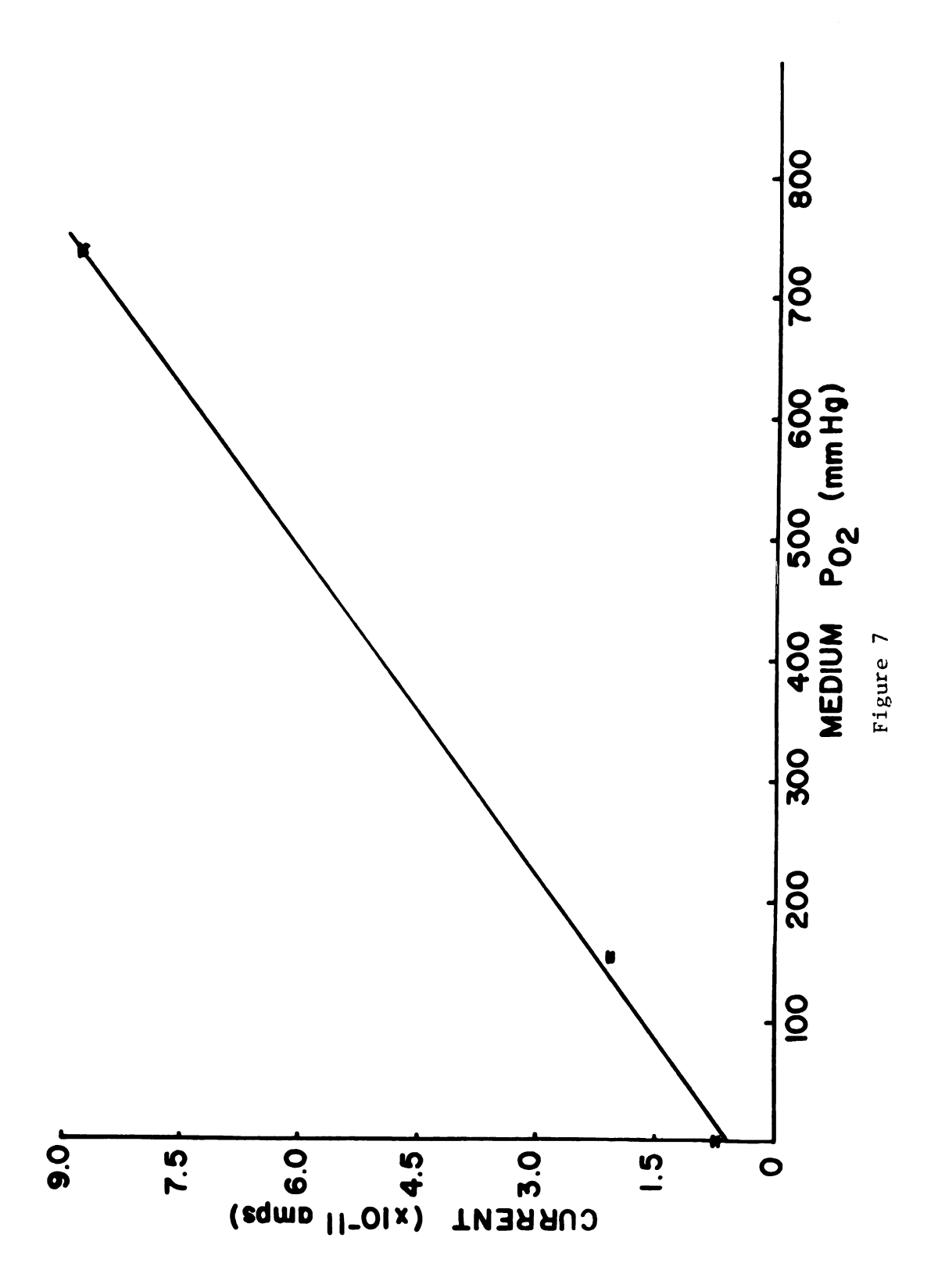


Figure 7. Effect of medium ${
m P}_{
m 0}$ on electrode

current. Data obtained in 154 mM

NaCl at 22C, and plotted as Mean +

Standard Error. $(r^2 = 0.998)$

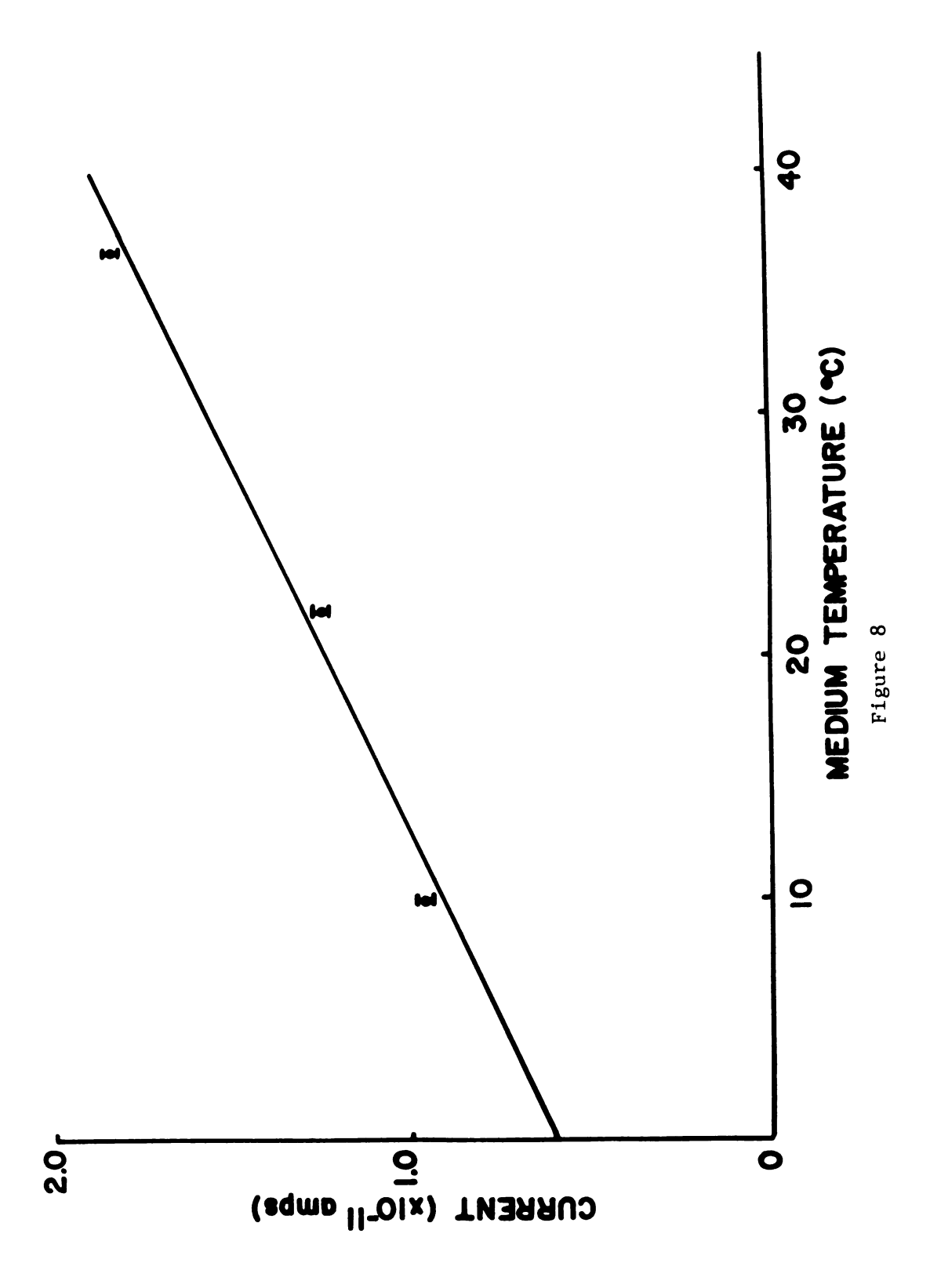


no	
temperature	
medium	
ot	
Effect	
Figure 8.	

154 mM NaCl at ~155 mmHg
$$(P_0)$$
, and

electrode current. Data obtained in

$$(\mathbf{r}^2 = 0.951)$$



Current vs. Salinity

Figure 9 shows a plot of electrode current vs. medium NaCl concentration. The slope of the regression line was found to be not significantly different from zero (p<0.05).

Electrode Stability

Results from the testing of electrode stability showed that the variation in current was less than 5% over a 2 h period when the electrode was placed in saline solutions saturated with either pure oxygen or air.

Current vs. Density

Results of the test of medium density on electrode current are shown in Figure 10. As the electrode was continuously driven ($\sim 5\mu/s$) into 2 g/dl agar, no discernable change in current was noted. This is in contrast to the results of Klinowski and Winlove (1980) who report a decrease in current as agar concentration is increased from 0.5 to 2 g/dl. Advancing the electrode through 5 g/dl agar resulted in a slight decrease in current, and a significant decrease occurred as the electrode reached the 7.5 g/dl agar layer.

Ocular Tissue Thicknesses

Retina - Mean retinal thickness was determined to be $324\pm3.3(242)~\mu$ [Mean \pm S.E.(N)]. The relative contribution of each of the retinal cell layers is shown in Figure 11, along with a picture and diagrammatic representation of the retina. A combined thickness value is reported for the interdigitating visual cell layer and pigmented epithelium layer.

Figure 9. Effect of medium salinity on

electrode current. Data obtained at

22C, 155 mmHg and plotted as Mean

+ Standard Error.

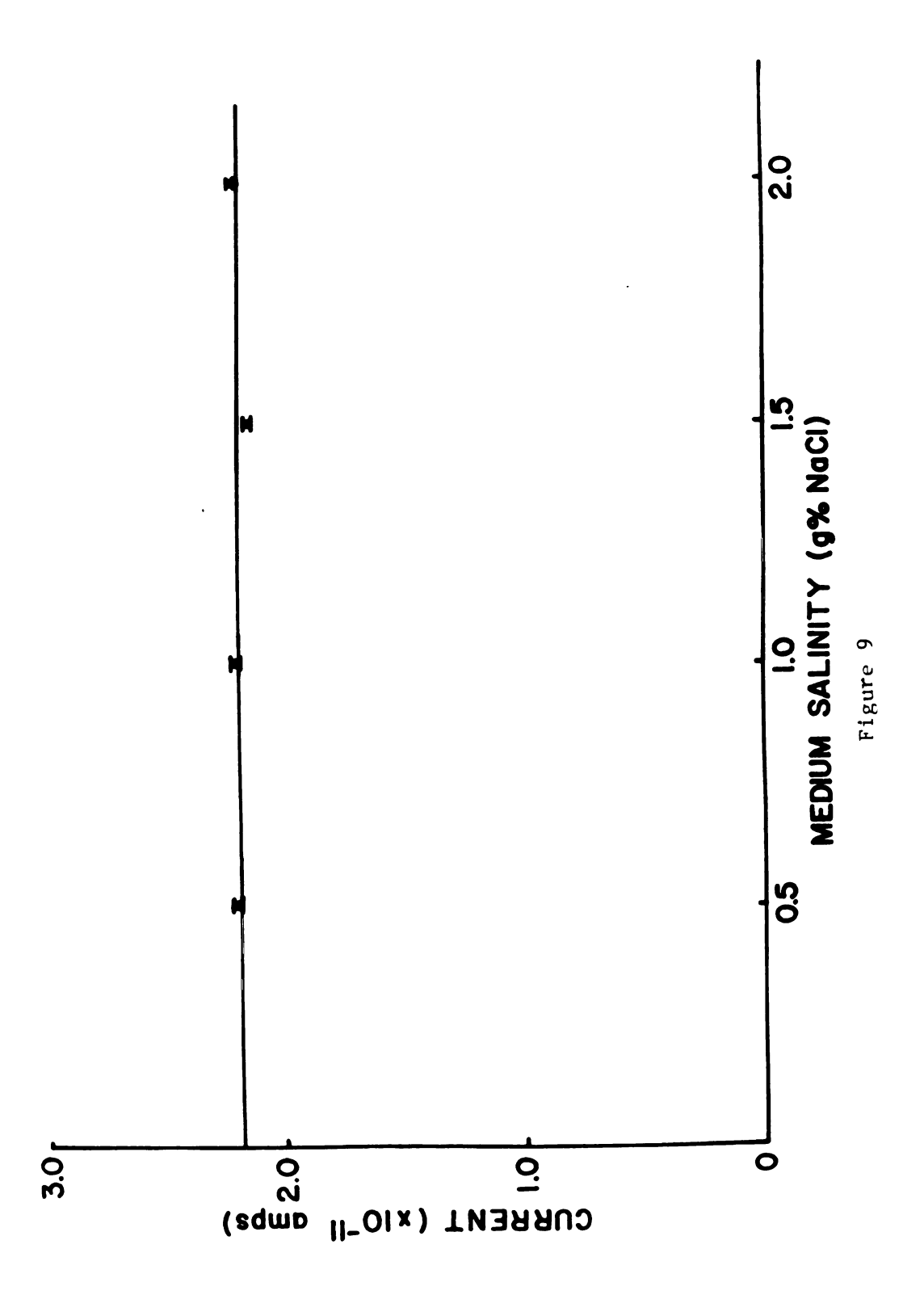


Figure 10. Effect of medium density on electrode current. This plot shows the current measured as the electrode was advanced through 154mM NaCl (22C; ~155 mmHg, P_{0}) followed by agar of differing concentrations. A corresponding diagram of the agar block is shown above the plot. Values shown indicate concentration of agar in grams/dl.

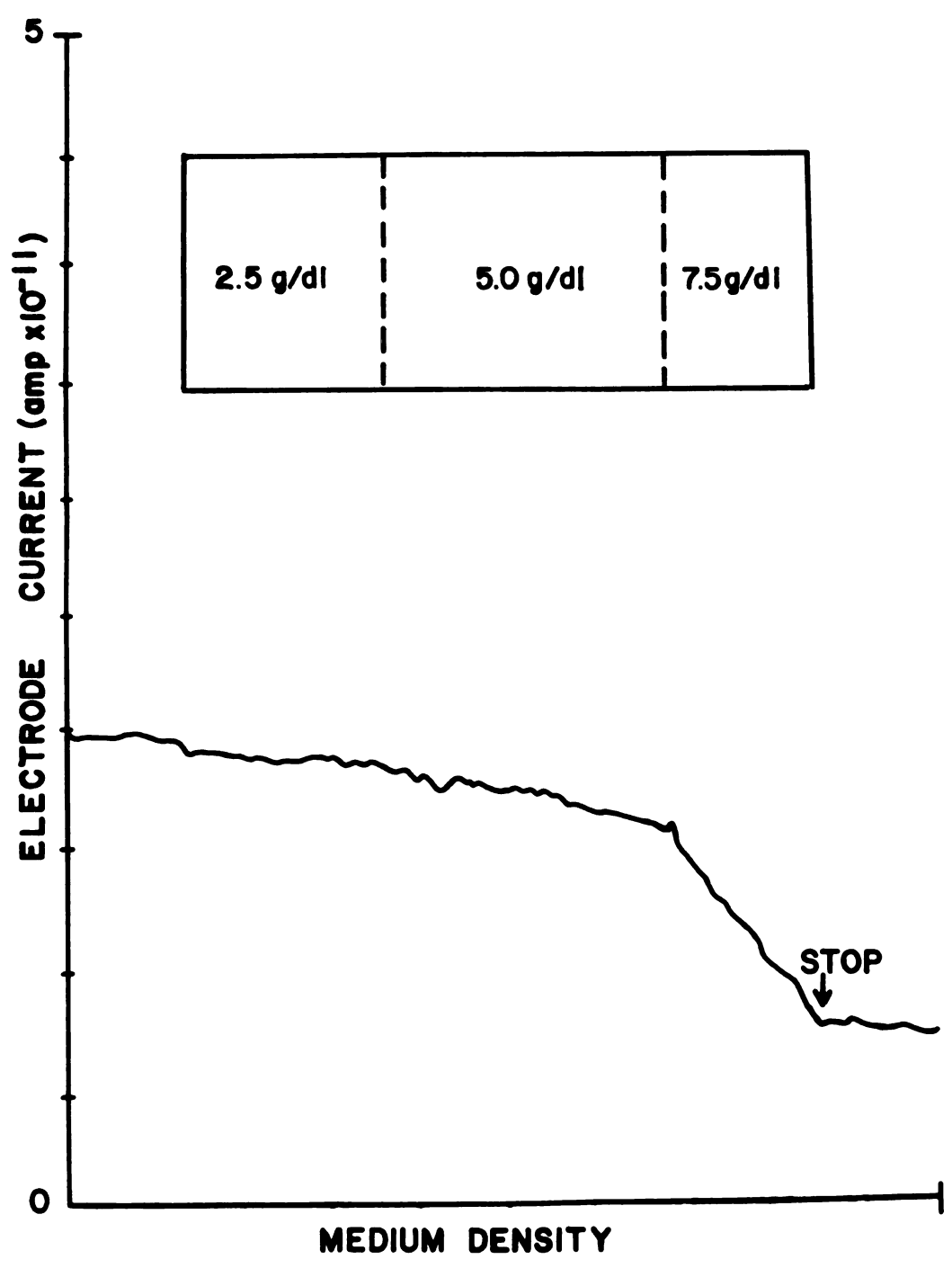


Figure 10

Figure 11. Mean thicknesses of retinal cell layers.

layers. This figure shows a diagram of the retinal cell layers above and a picture of the retina below. Mean retinal thickness was calculated to be 324.4. The relative contribution of each of the cell layers to the total retinal thickness is shown in the center box. (Picture from Ali and Anctil, 1976; diagram after Polyak,

GCL - Ganglion cell layer

IPL - Inner plexiform layer

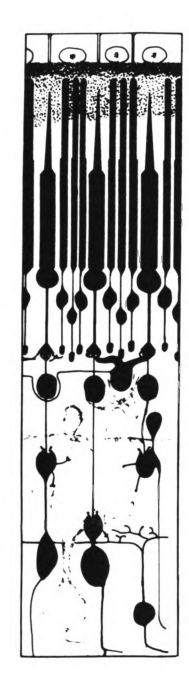
INL - Inner nuclear layer

OPL - Outer plexiform layer

ONL - Outer nuclear layer

VCL - Visual cell layer

PEL - Pigmented epithelium layer



			1207
200	7	INC OPLIONE	VCL/PEL
/0 2 01	11.00	1,000,000,000	70.05
8.0.9	80.5	U.U.74 (.U.74 G.D.76)	20.7%



Figure 11

Choroid - Figure 12 is a scale drawing of a transverse frozen section of a trout eye. Retinal and choroidal tissue thicknesses were determined along six possible axes of electrode penetration (labelled A through F in Figure 12). During each ocular P_{0_2} determination, the electrode was advanced in succession through the vitreous body, retina, distribution and collection vessels of the choriocapillaris, the choroid rete (axes B,C and D only), a stromatous space, and the sclera. Mean thicknesses of each respective tissue layer are shown in Table 1. The choriocapillaris is not totally distinguishable from the pigmented epithelium layer in frozen section, nor from the distribution and collection vessels in paraffin sections. The mean thickness of the choriocapillaris was estimated to be 20 μ .

In Vivo Ocular Po Profiles

A representative plot of the P_{0_2} profile measured through the retina and choroid of an individual trout eye is shown in Figure 13. A total of 19 ocular P_{0_2} profile determinations were made on the eyes of 19 different fish. The profiles characteristically showed an area of relatively low and constant P_{0_2} as the electrode was advanced through the vitreous (not shown in Figure 13), followed by an area where the P_{0_2} rapidly rises to a peak value. Mean maximum ocular P_{0_2} was determined to be $394\pm34(19)$ mmHg, and the maximum value recorded in any eye was 753.9 mmHg. As the electrode continued to advance, an area of much more variable P_{0_2} was encountered. The thickness of this area varied greatly from fish to fish and the P_{0_2} often showed very discrete, almost stepwise changes within this area. Further advancement of the electrode always resulted in a precipitous fall in P_{0_2} , to nearly 0 mmHg.

Figure 12. Diagram of possible axes of electrode penetration. This figure is a scale drawing of a transverse section of the trout eye. Labelled arrows indicate possible axes of penetration (see also Table 1).

RET - Retina

CRM - Choroidal rete mirabile

CC - Choriocapillaris

OM - Ocular muscle

ON - Optic nerve

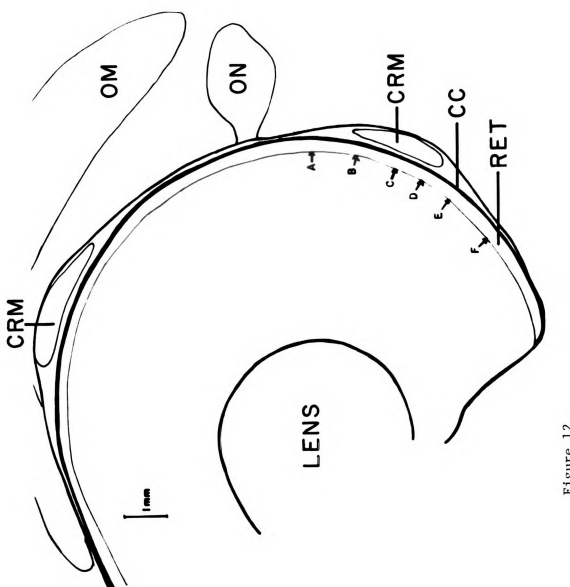


Figure 12

Table 1. Ocular tissue thicknesses.

PROFILE AXIS	RETINA	CHORIO- CAPILLARIS (µ)	DISTRIBUTION & COLLECTION VESSELS (µ)	RETE (µ)	STROMA	TOTAL (µ)
A :	339 <u>+</u> 14.0	20	178 <u>+</u> 16.1	0		521 <u>+</u> 16.0
В	348 <u>+</u> 15.0	20	90 <u>+</u> 7.7	306 <u>+</u> 19.7	73 <u>+</u> 6.1	831 <u>+</u> 29.1
C	329 <u>+</u> 13.6	20	78 <u>+</u> 5.8	515 <u>+</u> 28.9	59 <u>+</u> 5•4	987 <u>+</u> 38.6
D	336 <u>+</u> 12.9	20	76 <u>+</u> 5.9	461 <u>+</u> 21.1	60 <u>+</u> 3.6	936 <u>+</u> 38.3
E	342 <u>+</u> 9•9	20	344 <u>+</u> 18.6	0		700 <u>+</u> 23.5
F	313 <u>+</u> 10.8	20	132 <u>+</u> 15.6	0		455 <u>+</u> 25.6

ALL VALUES X+SE, N=18

Represents combined values for collection and distribution vessels and surrounding stroma.

Figure 13. Representative in vivo ocular \mathbf{P}_{02} profile. This figure shows a

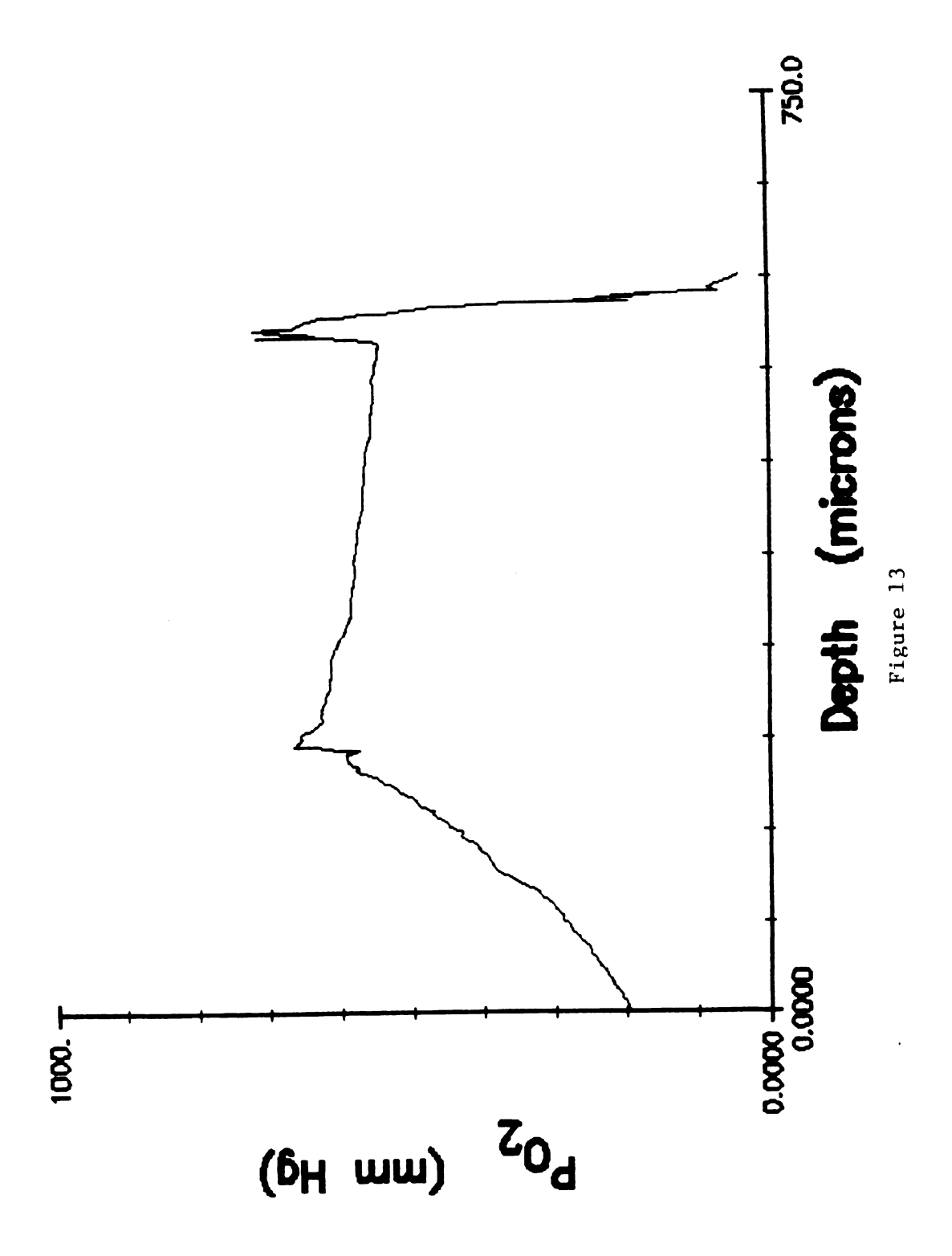
computer drawn plot of tissue oxygen

tension vs. depth of electrode

penetration through the retina and

choroidal layer. Data obtained at

9+0.50.



$\underline{\text{In}}\ \underline{\text{Vitro}}\ \underline{\text{Ocular}}\ \underline{P}_{0_2}\ \underline{\text{Profiles}}$

As the electrode was advanced in the anterior direction through the retina, the P_{0_2} rapidly decreased from the high P_{0_2} of the bath (~420 mmHg) to a much lower value as the vitreous body was reached (~32 mmHg). The mean P_{0_2} measured at the midpoint of each retinal cell layer is shown in Table 2.

Table 2. In vitro retinal $P_{0_{\stackrel{}{2}}}$ profile. Mean $P_{0_{\stackrel{}{2}}}$ calculated at the midpoint of each cell layer.

CELL LAYER	P _{O2} (mmHg)	
CHORIOCAPILLARIS	394 <u>+</u> 8.35(15)	
VISUAL CELL LAYER	288 <u>+</u> 7.08(14)	
OUTER NUCLEAR LAYER	229 <u>+</u> 3.24(4)	
OUTER PLEXIFORM LAYER	193 <u>+</u> 7.51(3)	
INNER NUCLEAR LAYER	152 <u>+</u> 7.78(3)	
INNER PLEXIFORM LAYER	110 ± 5.16(7)	
GANGLION CELL LAYER	85 <u>+</u> 2.50(7)	
VITREOUS BODY	32 <u>+</u> 3.93(31)	

MEAN+SE(N)

DISCUSSION

Po2 Microelectrodes

The microelectrode current in air-saturated saline $(2x10^{-11} \text{ amps})$ was comparable to that reported by Whalen et al. (1973), $(5x10^{-12} \text{ amps})$, who used an electrode identical in all respects except slightly smaller in diameter. Fatt (1964) demonstrated a linear relationship between current and medium P_{0_2} over the range of 0 to 150 mmHg. This finding was confirmed in the present study over a much wider range of medium Pos (O to 740 mmHg). The temperature coefficient of the electrodes used in this study (3.63%/C) was slightly higher than that reported by Fatt 1964), (2.5%/C). The dependence of electrode current on medium temperature necessitated the use of a refrigerated water bath which maintained the animal, saline medium and calibration media at a temperature constant to +0.5C. Thus the maximum error introduced by fluctuations in environmental temperature would be less than 4%. Response time of the electrodes (<2.5 s) was slightly longer than those of Whalen et al. (1973), who report response times <1 s. probably explained by the fact that their electrodes had a slightly shorter tip recess. In any event, the electrode was advanced through the eye in steps every 15 s, which was assumed to be adequate time for a steady-state current reading to be made. The electrode current remained stable in both air and 0, saturated saline for a period of 2 h, which is longer than the time required to obtain all of the in vitro P_{0_2} profiles, and most of the in vivo P_{0_2} profiles. The effect of medium density on electrode current is probably not due to physical pressure at the electrode tip, as it has been shown that a pressure of 200 psi results in only a 20% decrease in current (Fatt, 1964). Klinowski and Winlove (1980) reasoned that the decrease in current seen as the electrode penetrates dense agar is due to 0_2 consumption by the electrode, which results in a local depletion of oxygen. If the 0_2 diffusivity of the surrounding agar is low enough, the rate of diffusional supply of 0_2 to the electrode will not be high enough to maintain the electrode reduction current. It was assumed in this study that the 0_2 diffusivity of all ocular tissues, except the cartilagenous sclera, was sufficiently high to maintain the electrode current. In summary, the electrode response characteristics indicate that the 0_2 microelectrodes constructed for this study functioned effectively, and were well-suited for the measurement of tissue P_{0_2} .

In Vivo Ocular Pop Profiles

In order to further analyze the ocular P_{0} profiles obtained in vivo, it became necessary to determine precisely which portions of the profiles corresponded to each different tissue within the eye. Localization of the axis of electrode penetration was made possible by the marking electrode, but parallax error made it impossible to visualize the position of the electrode tip along the axis of penetration as it was advanced through the vitreous toward the retina. For this reason, it was assumed that the rapidly rising portion of the profile occurred as the electrode was advanced through the retina, and that the peak value of P_{0} was reached as the electrode penetrated the choriocapillaris. This fundamental assumption was based upon a number

of different factors, including both theoretical considerations and experimental evidence. These factors are listed below:

- Negishi et al. (1975) and Fairbanks (1968) report a very steep P_{0} gradient between the vitreous body and the choroidal layer of teleosts. They attribute this gradient to the high metabolic activity of the avascular retinas of these fish. A region of rapidly rising P_{0} would therefore be predicted as the retina was penetrated.
- The method for obtaining retinal P_{0_2} profiles in vitro allowed for direct visualization of the electrode tip as it first touched the choriocapillaris. Very close agreement exists between the in vitro retinal P_{0_2} profiles and the rising portion of the in vivo ocular P_{0_2} profiles.
- 3) The rapidly rising portion of the in vivo profiles always correlated closely with the measured mean retinal thickness (324 μ).
- 4) The current theory of countercurrent multiplication predicts that the highest ocular P_0 should occur with the vessels of the choriocapillaris. The half-life of the Root-off shift (unloading of O_2 from Hb and subsequent increase in choriocapillary blood P_0) has been reported to be <0.05 s, which is probably much faster than the amount of time required for blood to traverse the choriocapillaris.

The precipitous fall in P_{0_2} at the end of each in vivo profile is believed to be due to electrode penetration of the sclera. This belief is based upon correlation between the distance measured between the choriocapillaris and sclera, and the distance between the associated

points of each profile (specificially, the peak P_{0_2} and the rapid fall in P_{0_2}). It is reasoned that the microelectrode consumes a small amount of oxygen when in use, but that in most soft tissues the rate of 0_2 diffusion from the surrounding tissue is sufficiently high to maintain the oxygen current. Oxygen diffusivity in the very dense sclera however, is expected to be very low. If sufficiently low, then consumption of oxygen by the microelectrode will cause a local fall in tissue P_{0_2} , which 0_2 difusion is unable to rapidly compensate for and the result will be a decrease in the oxygen current "seen" by the electrode. Figure 14 shows the representative in vivo P_{0_2} plot (Figure 13) along with a diagram of the ocular tissues through which the electrode was advanced.

$\frac{\text{Retinal } P_{0}}{\text{In Vivo Profiles}}$

Mean choriocapillary P_{0_2} was calculated from the 19 profiles obtained in vivo and found to be $394\pm34(19)$ mmHg. This value does not significantly differ from the mean maximum ocular P_{0_2} [445 \pm 68(16) mmHg] reported by Fairbanks et al. (1969). This was interpreted as further indication that the 0_2 microelectrodes were functioning properly to measure P_{0_2} , as the data of Fairbanks et al. (1969) were obtained in the same species, but with an oxygen microelectrode of different design. Mean values of tissue P_{0_2} were also calculated for each 1 μ interval of distance from the vitreous body, through the retina to the choriocapillaris. Values of P_{0_2} at points where it was not actually measured, i.e., between each 10 μ sampling point, were interpolated. Figure 15 shows a plot of mean P_{0_2} vs. electrode depth through the retina. The corresponding retinal cell layers are diagrammed below the plot in

Figure 14. Representative in vivo ocular ${\bf P}_{0_2}$ profile with diagram of corres-

ponding ocular tissues. Diagram

drawn approximately to scale.

RET - Retina

CC - Choriocapillaris

DV - Distribution vessels

CV - Collection vessels

CRM - Choroidal rete mirabile

STR - Stroma

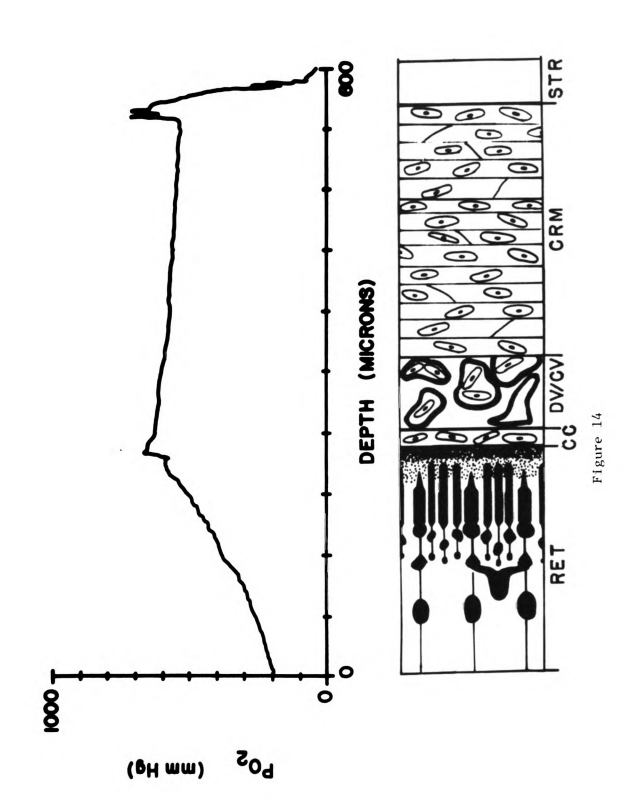
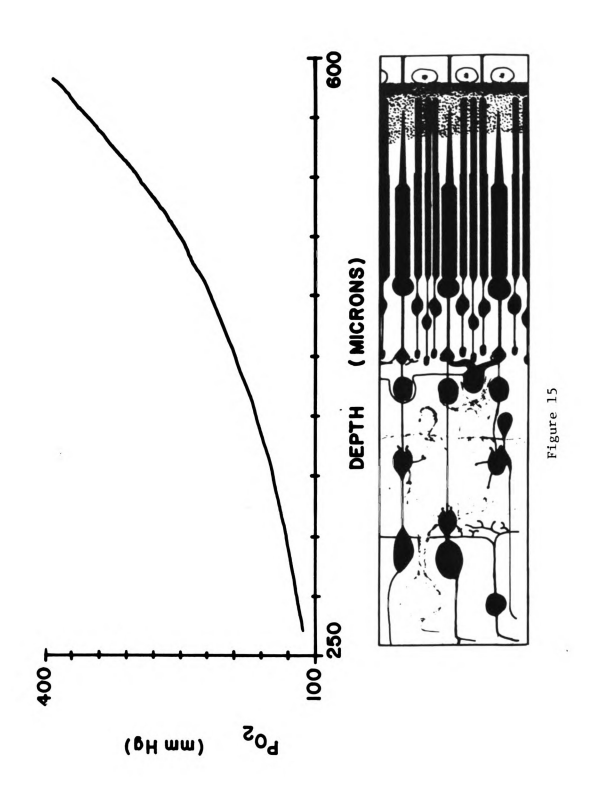


Figure 15. Retinal P₀ profile. This figure is a plot of mean retinal P₀ (calculated from the eyes of 19 fish) vs. depth of electrode penetration through the retina. Standard errors of these data ranged from 23 to 34 mmHg. A diagram of the retinal cell layers is shown below. (Diagram after Polyak, 1941).



The mean P_{0_2} at the retinal vitreous interface was calculated to be 113+23(11)mmHg, which also did not significantly differ from that reported by Fairbanks et al. (1969), [103+6.7(11)mmHg]. Thus, this study confirms that all retinal cell layers of the trout are normally exposed to oxygen tensions in excess of those found in the arterial blood [20+1.2(5) mmHg, Fairbanks et al., 1969]. More importantly, these data indicate that much of the trout retina, particularly the photoreceptors and pigment epithelial cells, are normally exposed to tissue oxygen tensions comparable to those known to exert toxic effects on the retinas of other species. The mean P_{0_0} at the midpoint of the photoreceptor-pigmented epithelium complex is 290+29(19) mmHg. Noell (1962) demonstrated that exposure of rabbits to 100% 0, at ambient barometric pressure results in widespread destruction of the photoreceptors. Exposure to 55% 0_2 at ambient pressure (P_{0_2} = 418 mmHg) resulted in similar effects if exposure was maintained for 7 days. It should be emphasized that the P_{0_2} at the tissue level, although not measured by these investigators, would be significantly lower than the exposure level, as P_0 would be expected to decrease as oxygen diffuses from the respiratory gas to the alveoli, the alveoli to the blood, and from the blood to the tissue. Thus it is reasonable to hypothesize that the trout retina and choroid must contain some means of resistance to the toxic effects of the high levels of oxygen to which they are continuously exposed.

In Vitro Profiles

The retinal P_{0_2} profiles obtained in vitro were characterized by a rapidly rising P_{0_2} gradient from vitreous body to choriocapillaris. The in vitro profiles were in very good agreement with the in vivo retinal

profiles lending further support to the assumption that peak ocular P_{0_2} occurs at the level of the choriocapillaris. Figure 16 shows a plot of both the in vivo and in vitro retina P_{0_2} profiles of the trout. The two profiles differed significantly only at the level of the vitreous body. The possible importance of this observation will be discussed later.

Analysis of the Retinal P_{0_2} Profile

After establishing that the P_{0_2} electrodes were functioning effectively, and determining the mean retinal P_{0_2} profile in vivo an attempt was made to mathematically characterize the retinal profile. The data were plotted as $ln(P_{O_2})$ vs electrode depth (Figure 17) in order to determine if the mean retinal P_{0} profile might be described by a multi-exponential function. The curve shown in Figure 17 was divided into six segments, each corresponding to one of the retinal cell layers, and the data in each segment tested by regression analysis. The slopes of the regression lines were tested against each other to determine the number of possible components of a multi-exponential function derived to fit the data. The slopes were found to be not significantly different from one another, with the exception of the visual cell and pigmented epithelium layer. This suggests that the mean retinal profile may be described by a two component exponential function. A computer curve fitting routine showed that the retinal profile was closely fit by the following equation:

$$P_{0_{2(x)}} = P_{0_{2(cc)}}(0.778e^{-0.0031x} + 0.222e^{-0.0161x})$$
 (8)

where: P_{0} = the oxygen tension of choriocapillaris blood in mmHg $_{2(cc)}$ = distance from the choriocapillaris in μ

Figure 16. Comparison of in vivo and in vitro retinal PO2 profiles. This plot shows the mean PO2 calculated at the midpoint of each retinal cell layer for both the in vivo (4) and in vitro (•) profiles.

Bars indicate standard error of the mean. The profiles differ significantly only at the level of the vitreous body.

VB - Vitreous body

GCL - Ganglion cell layer

IPL - Inner plexiform layer

INL - Inner nuclear layer

OPL - Outer plexiform layer

ONL - Outer nuclear layer

VCL - Visual cell layer

PEL - Pigmented epithelium layer

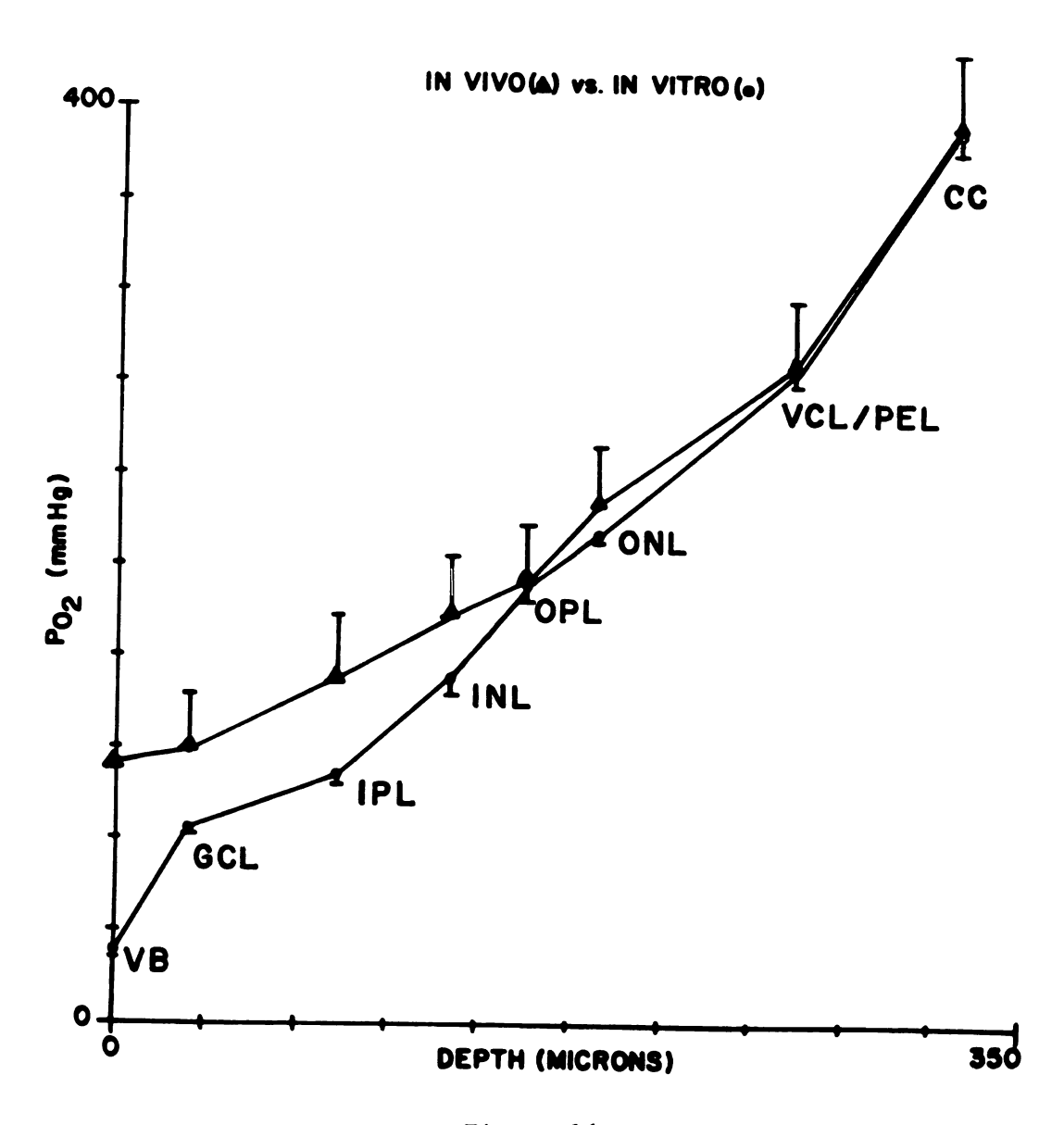
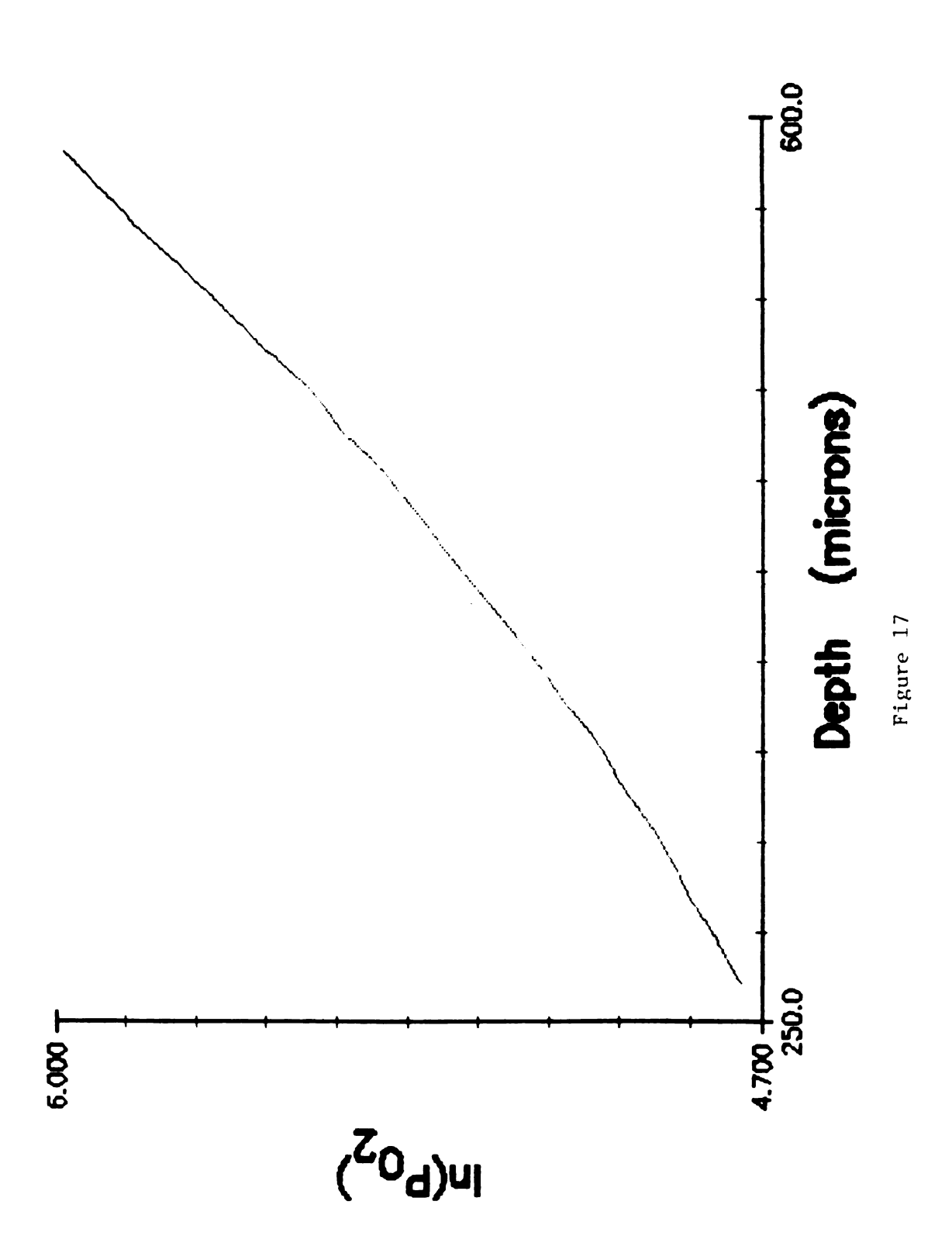


Figure 16

Figure 17. Plot of $\ln(P_0)$ vs. electrode position in the retins.



 $P_{\mbox{\scriptsize 0}}$ = the oxygen tension of the retina x μ from the choriocapillaris.

Equation (8) was generated with a curve fitting routine based upon ordinary least squares and the Gauss Minimization Method. The ordinary least squares variance estimate (sum of squared residuals) was equal to 17.2395. Table 3 shows the mean P_{0} measured at the midpoint of each retinal cell layer, along with the corresponding values predicted by equation (8). The maximum deviation of the predicted values from the measured values is less than 5% (Table 3).

The ability of equation (8) to predict the retinal P_{0_2} profile based on a different choriocapillary P_{0_2} was tested using the data of Fairbanks et al. (1969). These investigators were able to manipulate choriocapillary P_{0_2} by inhibiting the countercurrent oxygen multiplier mechanism of the choroidal rete with acetazolamide. With relatively large oxygen electrodes, Fairbanks et al. (1969) measured a mean choriocapillary P_{0_2} of 25±5.1(6) mmHg in acetazolamide treated rainbow trout and a mean vitreous body P_{0_2} of 7±1.0(6) mmHg. The P_{0_2} value predicted at the retinal vitreous interface by equation (8), (based upon a choriocapillary P_{0_2} of 25 mmHg and a retinal thickness of 324 μ) is 7 mmHg, precisely the value measured by Fairbanks et al.(1969).

Although equation (8) is useful as a predictor of the tissue P_{0} at any point within the retina of the trout, its derivation was completely empirical and it sheds little light on the nature of oxygen delivery and utilization within this tissue. For this reason, the data were subjected to an analysis similar to that used by Ganfield et al. (1970). Based upon the classical equations for one dimensional diffusion discussed earlier, the P_{0} distribution through the retina should also

Table 3. Comparison of the measured and predicted retinal P_{0_2} profiles. The predicted profile was obtained using the derived equation:

$$P_{02(x)} = P_{02(cc)} (0.778e^{-0.0031}x + 0.222e^{-0.0161x})$$
 where:

$$P_{02(cc)} = \text{the oxygen tension of the choriocapillary}$$

$$\text{blood in mmHg}$$

$$x = \text{distance from the choriocapillaris in } \mu$$

$$P_{02(x)} = \text{the oxygen tension of the retina } x \mu \text{ from } \mu$$

the choriocapillaris

CELL LAYER	MEASURED P _{O2}	P _O PREDICTED (mmHg)
CHORIOCAPILLARIS	394 <u>+</u> 34(19)	394
VISUAL CELL	290 <u>+</u> 29(19)	284
OUTER NUCLEAR	215 <u>+</u> 25(19)	209
OUTER PLEXIFORM	194 <u>+</u> 824(19)	189
INNER NUCLEAR	179 <u>+</u> 25(16)	171
INNER PLEXIFORM	153 <u>+</u> 27(13)	148
GANGLION CELL	120 <u>+</u> 24(11)	124

MEAN + SE(N)

be predicted by equation (6), if certain assumptions regarding the model hold. Specifically, oxygen consumption (V_{0_2}) , the diffusion coefficient (D) and the solubility coefficient (S) for oxygen must all be constant and independent of P_0 at all points within the retina. If these assumptions hold, then a plot of $(P_{0_{2(cc)}} - P_{0_{2(x)}})/x$ vs. x should yield a straight line. Figure 18 shows a plot of $(P_0 - P_0)/x$ vs. x for the mean retinal profile obtained in vivo. As illustrated in Figure 18, such a plot of the data does approximate a straight line. The slight deviation from linearity is probably due to small variations in v_{0} as the different retinal cell layers are penetrated. ficient of determination for these data (0.996) was interpreted as indicating that such variations in v_0 are not of sufficient magnitude to preclude estimation of the Krogh permeation coefficient. For the purposes of this analysis then, it was assumed that V_{0_2} , D, and S were all constant at each point in the retina. Since the slope of the line (Figure 18) equals $-V_{0_2}/2DS$ (equation 7), DS can be estimated based on a known value of V_{0_2} . The normal basal V_{0_2} of retinas isolated from Salmo gairdneri is 7.91 μ l 0₂/h mg protein at 15C, and 4.73 μ l 0₂/h mg protein at 10C (J.R. Hoffert, unpublished observations). Based on these data the temperature coefficient (Q_{10}) for trout retinal oxygen consumption was calculated to be 2.8. Using this value, the retinal oxygen consumption at 9C (the temperature at which the P_{0_2} profile was obtained) was calculated to be 4.264 µl 02/h mg protein. The slope of the regression line fit to the data in Figure 18 was calculated to be $-0.00311 \text{ mmHg/}\mu^2$. Thus:

 $^{-0.00311 \}text{ mmHg/}\mu^2 = (-0.00473 \text{ ml } 0_2/\text{h}^*\text{mg protein})/2DS$

Figure 18. Plot of transformed retinal data for the determination of the Krogh permeation coefficient. "P $_0$ " corresponds to the choriocapillary P $_0$ 2 in this study. "P $_0$ " corresponds to the P $_0$ measured at x μ from the choriocapillaris. Slope of the regression line fit to these data equals -0.00311 mmHg/ μ^2 . (r 2 = 0.996)

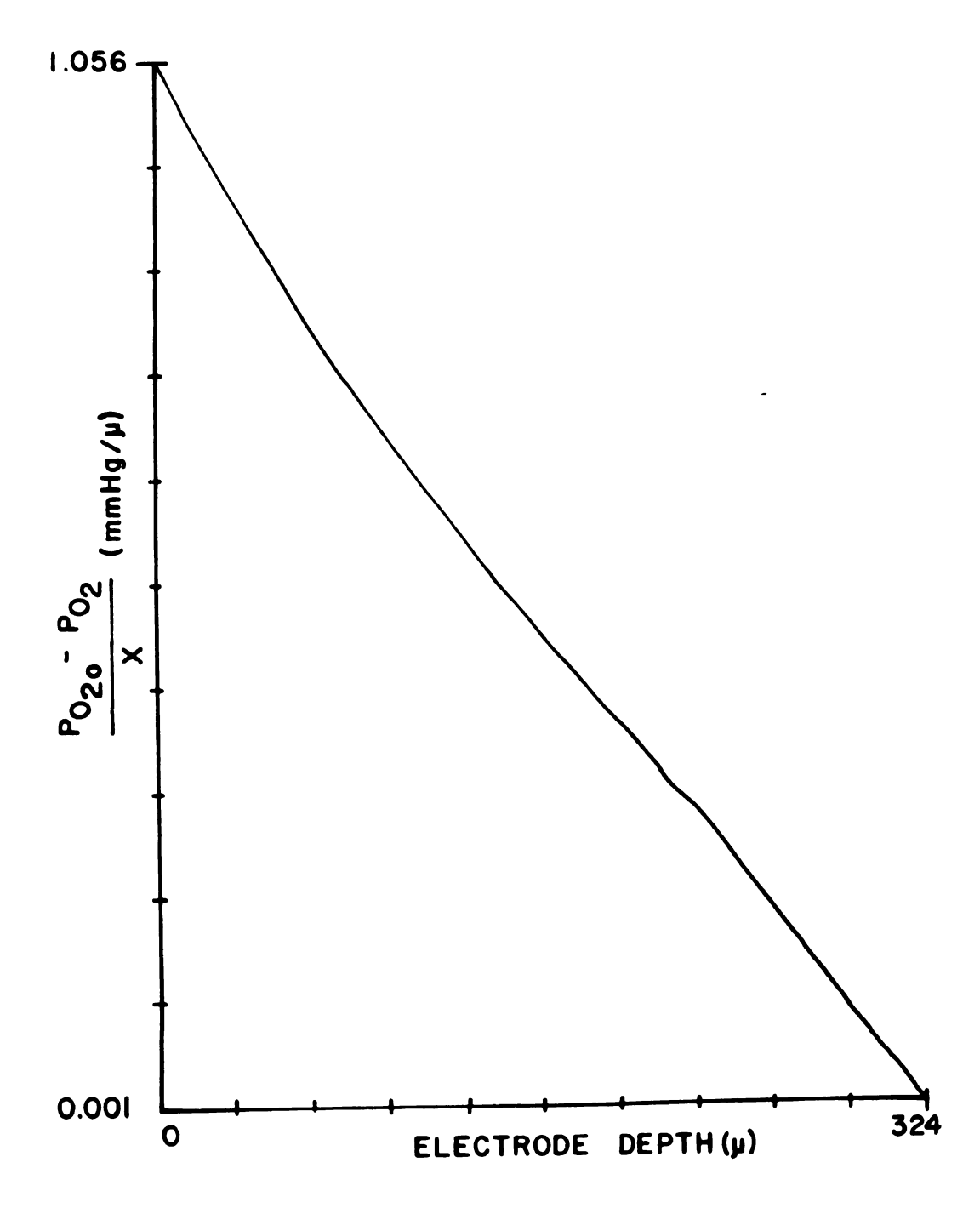


Figure 18

solving for DS (see Appendix II) yields:

DS = 6.70×10^{-6} ml $0_2/\text{min}^{\circ}\text{cm}^{\circ}\text{atm}$

It should be emphasized that this estimate of DS is based on data collected at 9C, and that the temperature dependence of DS should be taken into account when comparing the values obtained in different Ganfield et al. (1970) report a DS value of 1.29×10^{-5} studies. ml 0₂/min cm atm for cat cerebral cortex at 37C. Thews (1968) in a review of oxygen transport to tissue reports DS values ranging from 0.7 to 3.5×10^{-5} ml $0_{2}/\text{min}^{\circ}\text{cm}^{\circ}\text{atm}$ for a variety of species and tissues including skeletal muscle, cardiac muscle, cerebral cortex and plasma, all based on a temperature of 37C. (The values for the cerebral cortices of rabbit and rat were 1.9 and 2.1×10^{-5} ml $0_2/\text{min}^{\circ}\text{cm}^{\circ}\text{atm}$ respectively). Assuming a Q_{10} of 1.5, the DS value calculated for the retina of the trout may be corrected to 2.09×10^{-5} ml $0_2/min$ cm at 37C, a value well within the range reported by Thews (1968) and in very good agreement with the values reported for the neural tissue of other Tsacopoulos et al. (1981) report a DS value of 3.24×10^{-5} species. ml 02/min cm atm for the retina of the honeybee drone, Apis mellifera, measured at 22C. The corrected value for the trout is $1.13x10^{-5}$ ml 02/min cm at 22C. The difference between these two values may be explained in part by the high degree of structural dissimilarity between the retina of the trout and that of the drone.

SUMMARY AND CONCLUSIONS

- 1. A technique was devised and measurements made of normal intraretinal oxygen tensions of the rainbow trout in vivo using polarographic oxygen microelectrodes.
- 2. Retinal P_{0_2} increased from 113±23 mmHg at the retinal-vitreous body interface to 394±34 mmHg in the choriocapillaris. All cell layers of the trout retina were shown to be exposed to a P_{0_2} higher than that found in the arterial blood.
- 3. An equation was derived, based on the data, to predict the P_{0_2} distribution through the retina for any given choriocapillary P_{0_2} . The equation was shown to be accurate for predicting the retinal P_{0_2} profile at choriocapillary P_{0_2} values as low as 25 mmHg.
- 4. The P_{0} found in the trout retina is comparable to levels shown to cause toxicity in the retinas of other species. This finding indicates that the trout retina must contain some mechanism for protection against the mediators of oxygen toxicity.
- 5. Analysis of the P_{0_2} gradient showed that oxygen consumption is fairly uniform throughout the retinal cell layers of the trout under conditions of normal room light. This allowed for determiation of the Krogh permeation coefficient for oxygen within the trout retina.

RECOMMENDATIONS

Barriers to Oxygen Diffusion

The generation of high oxygen tensions in the trout eye is dependent upon discrete areas of high and low P_{0_2} . Specifically, the P_{0_2} should be highest in the peripheral end of the rete and choriocapillaris, and lowest at the central end of the rete - the point at which blood enters and exits the rete to the general circulation. The anatomic arrangement of the swimbladder and choroidal retia of the teleost is shown diagramatically in Figure 19. The spatial arrangement of the rete made it apparent during this study that some type of diffusion barrier is necessary to maintain maximum efficiency of the choroidal rete as an oxygen multiplier. If oxygen were allowed to diffuse across the relatively short distance from the choriocapillaris (high P_{0_2}) to the central end of the rete (low P_{0_2}), then the gradient driving diffusion of 0_2 from the efferent to the afferent capillaries would be destroyed, as would the lateral P_{0_2} gradient that exists along the retial The result would be a loss of oxygen to the general capillaries. circulation, and decreased efficiency of countercurrent multiplication.

Denton, Liddicoat and Taylor (1970,1972) have demonstrated the existence of "silvery" layers in the swimbladder walls of eels, that are 99% less permeable to oxygen than connective tissue. These

Figure 19. Anatomic arrangement of swimbladder and choroidal retia of the teleost. This figure contrasts the spatial arrangement of the respective retia. (A) Swimbladder rete; (B) Choroidal rete. Note the close proximetry of the retial capillaries to the choriocapillaris (high P_{O₂}) in the choroidal rete. It is hypothesized that a barrier to oxygen diffusion (indicated by the dashed line) must exist between the choriocapillaris and retial capillaries. (After Eckert and Randall, 1978).

CC - Choriocapillaris

DV - Distribution vessels

CV - Collection vessels

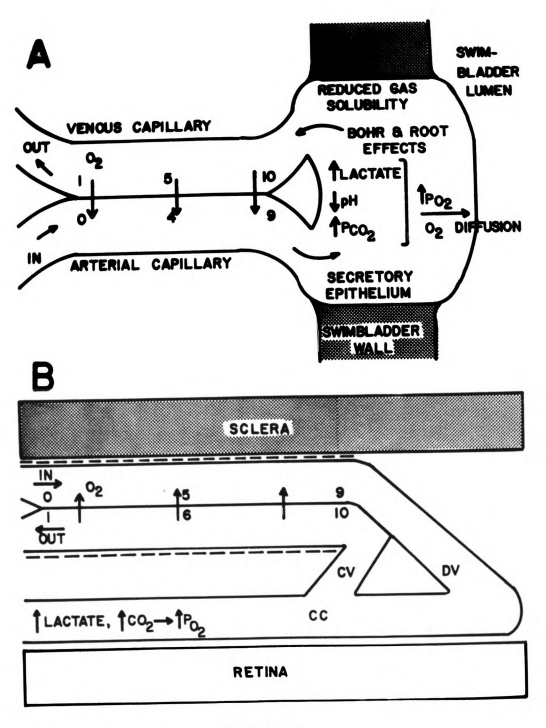


Figure 19

investigators find similar "silvery" layers surrounding the choroidal retia of some teleost species, and speculate that these layers may also serve as barriers to oxygen diffusion within the teleost eye. Examination of stained sections from paraffin-embedded eyes in this study revealed a discrete structure, brown in color, that surrounds and encapsulates the vessels of the trout choroidal rete. An attempt was made to correlate the anatomic location of this structure with any discontinuities in the choroidal P_{0_2} profiles. It was reasoned that if this layer did function as a barrier to oxygen diffusion, then profiles obtained along axes where the electrode penetrated the choroidal rete (axes B.C.D in Figure 12) especially the central end of the rete (axis B) would show very abrupt decreases in P_{0} from the choriocapillaris to the retial vessels. Several of the profiles obtained in vivo did show large discontinuities in P_{0_2} as the electrode penetrated the choroidal layer (See Figure 14). For several reasons, it was extremely difficult to correlate these with the precise location of the brown layer surrounding the rete. First, introduction of the marking electrode usually caused substantial hemorrhaging of the distribution, collection and retial vessels, which obscured the exact location of the boundries of the rete. Furthermore, the thickness of the rete varies greatly from the central to peripherial end. Small movements of the eye or experimental apparatus when inserting the marking electrode could cause relatively large errors in the estimation of retial thickness and the location of the brown layer. Nonetheless, these large discontinuities in the P_{0_2} profile are considered preliminary evidence for the existence of 0, diffusion barriers within the teleost eye, possibly of the type proposed by Denton et al. (1972). It is recommended that a more careful study of the structure and permeability characteristics of the layer surrounding the choroid rete be undertaken, to conclusively demonstrate that it is this structure that effectively acts to prevent diffusion of 0_2 into and out of the rete and consequent inhibition of the countercurrent multiplication effect.

Role of the Falciform Process in Retinal Oxygenation

Fairbanks et al. (1969) showed that unilateral pseudobranchectomy reduced the oxygen tension in the ipsilateral eye from 445 to 57 mmHg. They speculated that although pseudobranchectomy impaired the circulation in the choroidal rete mirabile, the lentiform body and falciform process circulation continued to elevate ocular P_{0_2} to levels in excess of the P_{0_2} of the arterial blood. This observation was based upon the mistaken description of lentiform body circulation given by Barnett (1951). As pointed out by Copeland (1980) a functioning choriocapillaris is required for elevation of Po, in the blood entering the falciform artery. Under conditions of normal choriocapillary blood flow however, the falciform process circulation should contain blood with relatively high P_{0_2} . The P_{0_2} in the vitreous body near the falciform process might therefore be expected to be higher than the P_{0} found at other points within the vitreous. Although no effort was made to control the precise location of electrode penetration in this study, it was noted that in certain profiles obtained in vivo the vitreous P_{0_2} decreased as the retinal surface was approached, suggesting that a source of oxygen exists at some point in the eye anterior to the retina. One possibility of such an oxygen source is the blood of the falciform process. Comparison of the in vivo and in vitro retinal profiles also revealed that the two mean profiles differed only at the level of the

vitreous body. A conceivable explanation for this observation is that after enucleation, the eye in vitro was supplied at the posterior surface of the retina with oxygen from the circulating bath, but the "internal" 0_2 supply (the falciform process) was lost. Thus, the falciform process may, under normal conditions, function to supply oxygen to the inner surface of parts of the trout retina. These results however are not conclusive. Another possible explanation of the observed results is that during the preparation of the animal for the in vivo profile determination, diffusion of oxygen from the saline bath increased the P_{0_2} of the vitreous at points near the corneal incision.

In order to further define the role of the falciform process circulation in retinal oxygenation, it is recommended that the P_{0_2} gradients in the vitreous body and retina, particularly in the area of the falciform process, be more carefully investigated.

LITERATURE CITED

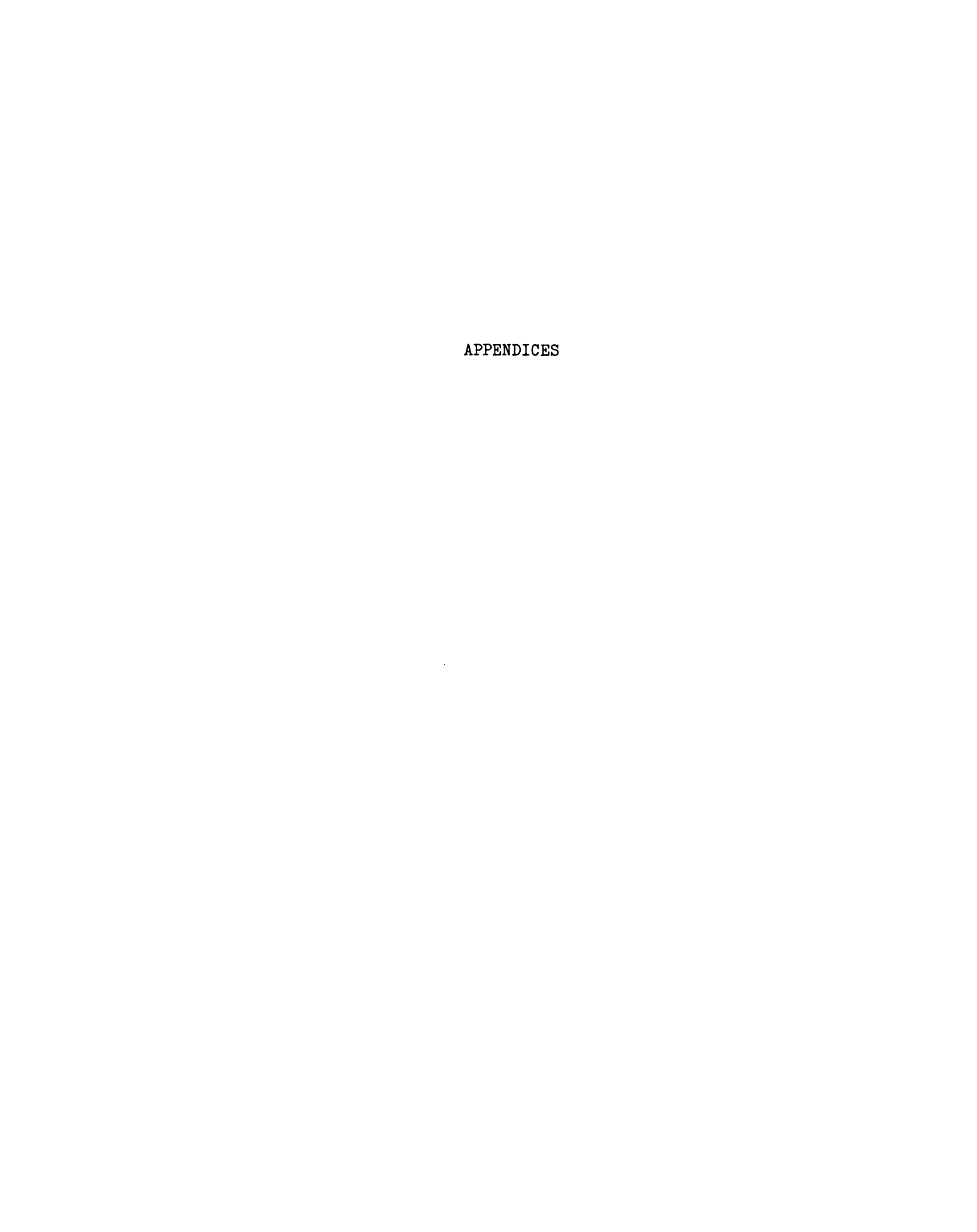
- Ali, M.A. and M. Anctil. 1976. Retinas of Fish. An Atlas. Springer-Verlag, NY, NY. 284p.
- Alm, A. 1972. Effects of norepinephrine, angiotensin, dihydroergotamine, papaverine, isoproterenol, histamine, nicotinic acid and xanthinol nicotinate on retinal oxygen tension in cats. Acta Ophthalmol., 50:707-718.
- Alm, A. and A. Bill. 1972. The oxygen supply to the retina, I. Effect of changes in intraocular and arterial blood pressures, and in arterial P_{O2} and P_{CO2} on the oxygen tension in the vitreous body of the cat. Acta Physiol. Scand., 84:261-274.
- Ashton, N. 1970. Some aspects of the comparative pathology of oxygen toxicity in the retina. Brit. J. Ophthal., 52:505-531.
- Ashton, N., B. Ward and G. Serpell. 1953. Role of oxygen in the genesis of retrolental fibroplasia. Brit. J. Ophthal., 52:505-531.
- Baeyens, D.A. and J.R. Hoffert. 1972. Inhibition of vertebrate retinal lactic dehydrogenase during exposure to normobaric oxygen. Aerospace Med., 43:263-265.
- Baeyens, D.A., J.R. Hoffert and P.O. Fromm. 1973. A comparative study of oxygen toxicity in the retina, brain and liver of the teleost, amphibian and mammal. Comp. Biochem. Physiol., 45A:925-932.
- Barnett, C.H. 1951. The structure and function of the choroidal gland of teleostean fish. J. Anat., 85:113-119.
- Berg, T. and J.B. Steen. 1968. The mechanism of oxygen concentration in the swimbladder of the eel. J. Physiol., 195:631-638.
- Berman, E.R. 1979. Biochemistry of the retinal pigment epithelium. In: The Retinal Pigment Epithelium. K.M. Zinn and M.F. Marmor, eds., Harvard University Press, Cambridge, MA. 521p.
- Bresnick, G.H. 1970. Oxygen-induced visual cell degeneration in the rabbit. Invest. Ophthal., 9:372-387.
- Clark, L.C., R. Wolf, D. Granger and Z. Taylor. 1953. Continuous recording of blood oxygen tensions by polarography. J. Appl. Physiol., 6:189-193.

- Copeland, D.E. 1951. Function of the glandular pseudobranch in teleosts. Am. J. Physiol., 167:775 (Abstract).
- Copeland, D.E. 1974a. The anatomy and fine structure of the eye of teleost: I. The choroid body in <u>Fundulus grandis</u>. Exp. Eye Res., 18:547-561.
- Copeland, D.E. 1974b. The anatomy and fine structure of the eye of teleost: II. The vascular connections of the lentiform body in Fundulus grandis. Exp. Eye Res., 19:583-589.
- Copeland, D.E. and D.S. Brown. 1976. The anatomy and fine structure of the eye in teleosts. V. Vascular relations of choriocapillaris, lentiform body and falciform process in rainbow trout (Salmo gairdneri). Exp. Eye Res., 23:15-27.
- Copeland, D.E. 1980. Functional vascularization of the teleost eye. In: <u>Current Topics in Eye Research</u>, Vol. 3. Academic Press, NY, NY. 336p.
- Davies, P.W. and F. Brink, Jr. 1942. Microelectrodes for measuring local oxygen tensions in animal tissues. Rev. Sci. Instru., 13:524-533.
- Davies, P.W. 1962. The oxygen cathode. Phys. Tech. Biol. Res., 4:137-139.
- Denton, E.J., J.D. Liddicoat and D.W. Taylor. 1970. Impermeable silvery layers in fish. J. Physiol., Lond., 207:64-65P.
- Denton, E.J., J.D. Liddicoat and D.W. Taylor. 1972. The permeability to gases of the swimbladder of the conger eel (Conger conger). J. Mar. Biol. Ass. U.K., 52:727-746.
- Drujan, B.D., G. Svaetichin and K. Negishi. 1971. Retinal aerobic metabolism as reflected in S-potential behavior. Vision Res. 3:151-159.
- Eckert, R. and D. Randall. 1978. Animal Physiology. W.H. Freeman and Company. San Francisco, CA. 558p.
- Fairbanks, M.B. 1968. Characterization of the normal ocular oxygen tension in the eye of rainbow trout (Salmo gairdneri) using a microoxygen polarographic electrode. M.S. Thesis. Michigan State University. East Lansing, MI.
- Fairbanks, M.B., J.R. Hoffert and P.O. Fromm. 1969. The dependence of the oxygen-concentrating mechanism of the teleost eye (Salmo gairdneri) on the enzyme carbonic anhydrase. J. Gen. Physiol., 54(2):203-211.

- Fairbanks, M.B. 1970. The importance of the enzyme carbonic anhydrase in ocular oxygen concentration in the rainbow trout (Salmogairdneri). Ph.D. Thesis. Michigan State University. East Lansing, Michigan.
- Fairbanks, M.B., J.R. Hoffert and P.O. Fromm. 1974. Short circuiting the ocular oxygen concentrating mechanism in the teleost Salmo gairdneri using carbonic anhydrase inhibitors. J. Gen. Physiol. 64:263-273.
- Fange, R. 1953. The mechanisms of gas transport in the euphysoclist swimbladder. ACTA Physiol. Scand., 30:1-133.
- Fatt, I. 1964. An ultramicro oxygen electrode. J. Appl. Physiol., 19:326-329.
- Fatt, I. 1969. The steady state distribution of oxygen and nitrogen in the in vivo cornea. II. The open eye in nitrogen and the covered eye. Exp. Eye Res., 7:413-430.
- Fatt, I. 1976. Polarographic Oxygen Sensors. CRC Press, Cleveland, OH. 278p.
- Fatt, I. and M.T. Bieber. 1969. The steady state distribution of oxygen and carbon dioxide in the in vivo cornea. I. The open eye in air and the closed eye. Exp. Eye Res., 7:103-112.
- Fonner, D.B., J.R. Hoffert and P.O. Fromm. 1973. The importance of the countercurrent oxygen multiplier mechanism in maintaining retinal function in the teleost. Comp. Biochem. Physiol., 46A:559-567.
- Forster, R.E. and J.B. Steen. 1969. The rate of the 'Root shift' in the eel red cells and eel haemoglobin solutions. J. Physiol., 204:259-282.
- Frank, L. and D. Massaro. 1980. Oxygen toxicity. Am. J. Med., 69:117-126.
- Fridovich, I. 1970. Quantitative aspects of the production of superoxide anion radical by milk xanthine oxidase. J. Biol. Chem., 245(16):4053-4057.
- Fridovich, I. 1977. Oxygen it toxic! Bioscience, 27:462-466.
- Ganfield, R.A., W.J. Whalen and P. Nair. 1970. Mass transfer, storage and utilization of O₂ in cat cerebral cortex. Am. J. Physiol., 219:814-821.
- Haldane, J.S. 1922. Respiration. University Press, New Haven, CT. 682p.
- Hill, A.V. 1928. The diffusion of oxygen and lactic acid through tissues. Proc. R. Soc. Lond. B. Biol. Sci., 104:39-96.

- Hoffert, J.R. and J.L. Ubels. 1979. The intraocular P_{O2} and electroretinogram of the trout as affected by temperature and ventilatory flow. Comp. Biochem. Physiol., 62A:563-568.
- Klinowski, J. and C.P. Winlove. 1980. Artifacts in the polarographic measurement of oxygen tension in tissue. J. Physiol. 303:84P.
- Kuhn, W., A. Ramel, H.J. Kuhn and E. Marti. 1963. The filling mechanism of the swimbladder. Generation of high gas pressures through hairpin countercurrent multiplication. Experientia, 19:497-552.
- Lucas, D.R. and O.A. Trowell. 1958. In vitro culture of the eye and the retina of the mouse and rat. J. Embryol. Exptl Morph., 6:178-182.
- Maetz, J. 1953. L'Anhydrase Carbonique dans deux Teleosteans Varions. Comparaison des Activites Anhydasiques chez Penca et Seranus. Compt. Rend. Soc. Biol., 147:204-206.
- Negishi, K., G. Svaetichin, M. Laufer and B. D. Drujan. 1975. Polarographic and electrophysiological studies of retinal respiration. Vis. Res., 15:527-533.
- Noell, W. 1962. Effect of high and low oxygen tension on the visual system. In Schaeffer, K.E., Ed., Environmental Effects on Consciousness. Macmillian, New York. pp 3-18.
- Patz, A., L.E. Hoeck and E. De La Cruz. 1952. Studies on the effect of high oxygen administration in retrolental fibroplasia: nursery observations. Am. J. Ophthal., 35:1248-1253.
- Polyak, S. 1941. The Retina. University of Chicago Press, Chicago, IL. 601p.
- Santamaria, L., B.D. Drujan, G. Svaetichin and K. Negishi. 1971. Respiration glycolysis and s-potentials in teleost retina: a comparative study. Vis. Res., 11:877-887.
- Shaw, A.M. and H.A. Leon. 1970. Retinal dehydrogenases in rabbits exposed to 100 percent oxygen. Aerospace Med., 41:1055-1060.
- Schneiderman, G. and T.K. Goldstick. 1975. Oxygen fields induced by recessed and needle oxygen microelectrodes in homogeneous media. Adv. Exp. Med. Biol., 75:9-16.
- Takahashi, G.H. and I. Fatt. 1965. The diffusion of oxygen in the cornea. Exp. Eye Res., 4:4-12.
- Takahashi, G.H., I. Fatt and T.K. Goldstick. 1966. Oxygen consumption rate of tissue measured by a micropolarographic method. J. Gen. Physiol., 50:317-335.

- Thews, G. 1968. The theory of oxygen transport and its application to gaseous exchange in the lung. In: Oxygen Transport in Blood and Tissue. D.W. Lubbers, U.C. Luft, G. Thews and E. Witzleb, eds., Georg Thieme Verlag, Stuttgart. 264p.
- Tsacapoulos, M., S. Poitry and A. Borsellino. 1981. Diffusion and consumption of oxygen in the superfused retina of the drone (Apis mellifera) in darkness. J. Gen. Physiol., 77:601-628.
- Ubels, J.L., J.R. Hoffert and P.O. Fromm. 1977. Ocular oxygen toxicity: The effect of hyperbaric oxygen on the in vitro electroretinogram. Comp. Biochem. Physiol., 57A:29-32.
- Ubels, J.L. and J.R. Hoffert. 1981. Ocular oxygen toxicity: The effect of hyperbaric oxygen on retinal Na K ATPase. Exp. Eye Res., 32:77-84.
- Whalen, W.J., J. Riley and P. Nair. 1967. A microelectrode for measuring intracellular P_{02} . J. Appl. Physiol., 23:798-801.
- Whalen, W.J., P. Nair and R.A. Ganfield. 1973. Measurements of oxygen tension in tissues with a micro oxygen elctrode. Microvasc. Res., 5:254-262.
- Wittenberg, J.B. and B.A. Wittenberg. 1961. Active transport of oxygen and the eye of fish. Biol. Bull., 121:379.
- Wittenberg, J.B. and B.A. Wittenberg. 1962. Active secretion of oxygen into the eye of fish. Nature (London), 194:106-107.
- Yanoff, M., W. Miller and J.A. Waldhausen. 1970. Oxygen poisoning of the eyes. Comparison of cyanotic and acyanotic dogs. Arch. Ophthal., 84:627-629.
- Zuckerman, R. and J.J. Weiter. 1980a. Oxygen transport in the bullfrog retina. Exp. Eye Res., 30:117-127.
- Zuckerman, R. and J.J. Weiter. 1980b. Oxygen transport in the bullfrog retina. A reply. Exp. Eye Res., 30:727-728.



APPENDIX I

Composition of Buffered Ringer Solution

NaCl	8.00g	137.7mM
KCl	0.20g	2.7mM
Na ₂ HPO ₄	1.15g	8.1mM
KH2PO4	0.18g	1.3mM
CaCl ₂	0.10g	0.9mM
MgCl ₂ • 6H ₂ 0	0.19g	0.3mM
^C 6 ^H 12 ^O 6	1.00g	5.6mM
Distilled H ₂ 0	To 1 liter	

APPENDIX II

Calculation of Krogh Permeation Coefficient

1.
$$v_{0_2} = 4.264 \text{ } \mu l \text{ } 0_2/h^*mg \text{ protein } @ T = 9C \text{ (See text)}$$

- 2. Slope of plot from Figure 18 = -0.0031 mmHg/ μ^2 (See text)
- 3. Assume: Protein = 7.7% of retinal wet weight (Berman, 1979) 1 g wet tissue = 1 cm³wet tissue

4. Then:
$$v_{0_2} = 5.47 \text{ } \mu l \text{ } 0_2/\text{min} \cdot \text{cm}^3 \text{ } @ \text{ } T = 90$$

$$= \frac{-0.00547 \text{ ml } 0_2/\text{min}^{\circ}\text{cm}^3}{2(-0.00311 \text{ mmHg/}\mu^2)} = 0.882 \frac{\text{ml } 0_2^{\circ}\mu^2}{\text{min}^{\circ}\text{cm}^3 \cdot \text{mmHg}}$$

6. DS = 0.882
$$\frac{\text{ml } 0_2 \cdot \mu^2}{\text{min cm}^3 \cdot \text{mmHg}} \times 760 \frac{\text{mmHg}}{\text{atm}} \times \frac{1}{(10,000)^2} \frac{\text{cm}^2}{\mu^2}$$

= 6.70 x 10⁻⁶ $\frac{\text{ml } 0_2}{\text{min cm}^3 \cdot \text{atm}}$